UCLouvain

École polytechnique de Louvain

Comparative LCA of supply strategies for forest-monitoring IoT sensor networks

Author: **Aurélien Buxant**
Supervisor: **David Bol**
Readers: **Denis Flandre**, **Marco Gonzalez**, **Augustin Wattiez**, **Jona Cappelle**
Academic year 2023–2024
Master [120] in Mechanical Engineering

Abstract

Forest fires are becoming more frequent and, in the context of climate change, their mitigation is a necessity to prevent significant greenhouse gas emissions into the atmosphere. Their impact extends beyond the environmental sphere, with economic and human health consequences. Many techniques are currently being implemented to monitor forest fires with an active scientific literature on this topic, and remote sensing relying on IoT devices offers a promising solution for continuous monitoring and early warning of fire hazards. However, the solution must not become part of the problem. The purpose of this work is to compare three existing energy sources available for IoT devices, (1) solar energy harvesting, (2) battery power and (3) recharging via Unmanned Aerial Vehicles (UAVs). The cradle-to-gate Life-Cycle Assessment (LCA) approach is used to assess the environmental impact of the sensor and the energy sources, considering a 10-year use phase. The comparison is based on a common topology using a sensor inspired by the product of Dryad Networks GmbH, adapted to the need of each energy source. The system studied involves the deployment of 80 sensors to cover the area around one kilometre of road in a forested area, within a radius of 2 km. The studied system of 80 sensors emits 504 kg CO2e when powered by batteries, 270 kg CO2e when recharged by UAVs and 154 kg CO2e when relying on solar cells. Several impact categories are analysed. Across all of them, the battery system is more impactful than the solar system and the UAV system. Apart from the GWP, the lower difference is a factor of 9.55 between the estimated impacts of the battery system and the solar system, for the freshwater eutrophication. The higher difference is a factor of 700 between the estimated impacts of the battery solution and the solar solution for the cancerous effects on human health. When compared to the potential CO2 emissions of forest fires, the use of such remote sensing systems seemed fully justified. However, in terms of planetary boundaries, the battery and UAV options raise concerns. If all the world's forests were to be covered, their impact on the cancerous and non-cancerous effects would reach 4.7% and 1.39% of the planetary boundaries for the battery, and 0.42% and 0.13% for the UAV solution. The UAV has potential, but the way in which its use phase is modelled needs further investigation for it to provide robust conclusions.

Acknowledgements

This work would never have seen the light of day without the invaluable help of many people, whom I would like to thank here.

First of all, I am grateful to my supervisor, Prof. David Bol, for including me in his project. As a MECA student, this field of research was brand new to me and his support, guidance and encouragement were of great help to explore this meaningful subject. I would also like to thank him for his regular monitoring of the progress of my work.

I also want to thank Augustin Wattiez, Marco Gonzalez and Jona Cappelle for their availability and advices. I had a lot to learn and their insights helped me a lot in the completion of this work.

And at last, I thank my parents for their support throughout these six years.

Contents

Nomenclature

AP	Acidification potential
BoM	Bill of Materials
DISC	Double side contacted cells with innovative carrier-selective contacts
Dryad	Dryad Networks GmbH
EF 3.0	Environmental Footprint 3.0
EoL	End-of-Life
FEP	Freshwater eutrophication
FETP	Freshwater ecotoxicity
GWP	Global Warming Potential
HJT	Heterojunction Technology
HOFP	Photochemical ozone formation, human health effects
HTPc	Human toxicity, cancer effects
HTPnc	Human toxicity, non-cancer effects
IC	Integrated Circuit
ILCD	International Reference Life Cycle Data
IoT	Internet-of-Things
LCA	Life-Cycle Assessment
LCI	Life-Cycle Inventory
LCIA	Life-Cycle Impact Assessment
LCIA	Life-Cycle Impact Assessment
LoRaWAN	Long Range Wide Area Network
LTC	Lithium/thionyl chloride
LTO	Lithium-titanium-oxide

MCU	Microcontroller Unit
MET	Maritime eutrophication
mono-Si	Monocrystalline silicon
multi-Si	multicrystalline Silicon
NDA	Non-Disclosure Agreement
ODP	Ozone depletion potential
PB	Planetary boundaries
PCB	Printed Circuit Board
PERC	Passivated Emitter and Rear Contact
PM	Particulate Matter
PM10	Particulate Matter with $\varnothing < 10$ µm
PM2.5	Particulate Matter with $\varnothing < 2.5$ µm
PMU	Power Management Unit
poly-Si	Polycrystalline silicon
PV	Photovoltaic
RX	Receiver
SC	Supercapacitor
SOP	Resource use, mineral and metals
TEP	Terrestrial eutrophication
TX	Transmitter
UAV	Unmanned Aerial Vehicle
WCP	Water use
WPT	Wireless Power Transfer

List of Figures

List of Tables

Introduction

Context

Since ancient times beyond the creation of cuneiform writing, the acrid smell of smoke replacing the petrichor[1] in a forest meant renewal, improvement, cleansing and fertilizing for the ecosystem [2].

But until recently, forest fires, also known as wildfires, have been less frequent and less intense. At a time when forest fires are becoming more frequent, it is imperative that people, companies, and countries are equipped with weapons to fight them. Forest fires are devastating for many reasons. They destroy ecosystems, kill wildlife and people, and require expensive resources to fight [3][4]. One way to combat them is to stop them before they spread and do not require huge resources to fight. This can be done by using sensor networks in the endangered forests to detect changes in atmospheric conditions such as CO_2 concentration, pressure, temperature, and humidity [5].

But one should be careful that the solution is not worse than the problem it tries to solve. IoT sensor networks are widespread throughout the world, with 15.9 billion devices deployed in 2023 [6]. This implies that their operating system is well known. However, the question of which energy supply must be employed has still found no decisive answer [7]. And this question is even more prevalent in forest monitoring, as IoT devices are placed in remote locations.

Using Life-Cycle Assessment (LCA) methodology, it is possible to compare different energy sources to determine which is less damaging to the environment. The results can then be used as a decision support tool for a designer when developing a sensor network.

[1]"The smell produced when rain falls on dry ground, usually experienced as being pleasant." Definition from the Cambridge Advanced Learner's Dictionary & Thesaurus © Cambridge University Press[1]

Objectives

The aim of this study is to develop a model to compare multiple energy sources and, if possible, create a hierarchy between them. It will be applied to forest monitoring and the conclusions will be directed to this use case. The conclusions may vary from case to case.

It also aims to assess the environmental footprint of the sensor industrially produced by Dryad Networks GmbH, the Wildfire sensor [5].

The results are contextualised with two different references. First, with the planetary boundaries and then with the emissions from a forest fire.

Structure

The document is structured into four chapters. The first chapter provides the context for the study, outlining the environmental, economic and human health impacts of forest fires, offering a comprehensive overview of the technologies employed in forest monitoring, explaining how IoT nodes function and communicate, and finally, digging into the specifications of the three energy sources studied in this thesis. The second chapter summarises the results of previous work on assessing the environmental impacts of IoT nodes used in remote sensing. The third chapter describes the LCA methodology used in this work and develops in detail how it has been applied here. The fourth chapter interprets the results obtained, contextualises them and discusses possible ways of improving each solution.

The use of AI, via DeepL write, in this document has been limited to improving the form of what the author writes to make the text more correct and pleasant to read, given that he is not a native English speaker.

Chapter 1

Background Information

The aim of the first chapter is to give the reader a quick overview of the context of this study, in order to explain its motivation, using a top-down approach as shown in Figure 1.6. Firstly, it will explore the different impacts of a forest fire on the environment. Secondly, it will give an overview of the different techniques used to monitor forests and how they can be effective in predicting forest fires. Third, it will review the architecture of the Internet-of-Things (IoT) nodes used in a remote sensing application. Fourth, a quick explanation of the Long Range Wide Area Network (LoRaWAN) and how it works will be given. Finally, a fifth section will present all the energy sources available to an IoT node, with a brief explanation of how they work.

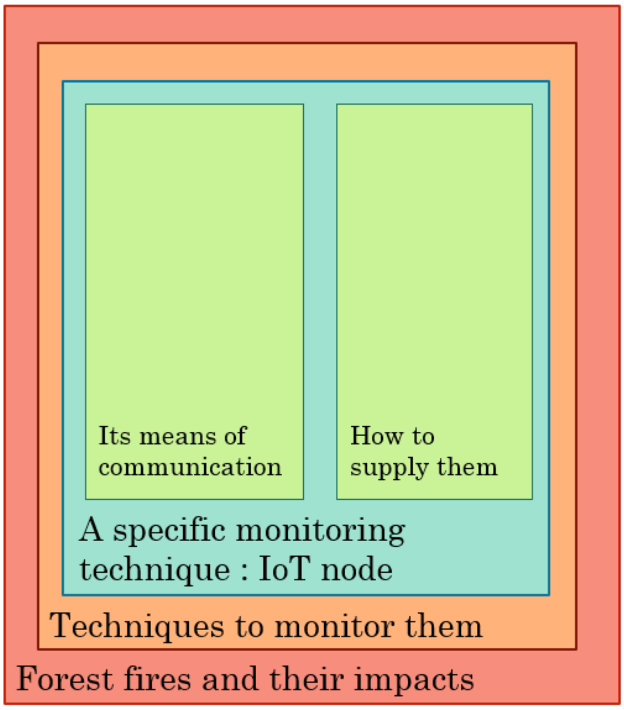

Figure 1.1: A top-down overview of the study's context.

1.1 Forest Fires Impacts

Forest fires, often referred to as vegetation fire or wildfires, have garnered increased attention in recent years due to their growing frequency, intensity, and severity.

This natural phenomenon can be both advantageous and detrimental for the environment. On one hand, forest fires have occurred for hundreds of millions of years, and many ecosystems have adapted to them; some even require fires to thrive. When controlled by humans, they can also be highly effective for clearing agricultural land, as well as for fire prevention and management. Controlled burns, for instance, create breaks in the landscape that reduce fuel for wildfires and interrupt potential fire spread pathways [8].

However, uncontrolled wildfires that occur too often lead to destruction, loss of life, biodiversity, and are regarded as environmental disasters [9]. Therefore, the monitoring of forests is crucial to predict and mitigate such disasters. Various techniques exist in this field, which will be broadly discussed in the following section.

Before delving into specifics, let's briefly examine the causes of wildfires. In the state of California, USA, 95% of fires are believed to be started by humans. From unattended campfires to discarded cigarettes in wilderness areas, numerous human actions can trigger forest fires [10]. A similar proportion is observed in Mediterranean forests, but the percentage, 87%, is lower in boreal forests. Aside from human causes, another potential ignition source is lightning, under the right conditions, such as a positively charged cloud-to-ground lightning strike on an inflammable object [11][12].

In both human-caused and natural cases, three elements are necessary for a fire to ignite: fuel, oxygen, and a heat source. Dry weather, drought, and strong winds further contribute to creating ideal conditions for a smouldering fire to escalate into a blaze spanning multiple kilometres [10].

Now that this has been covered, let's explore the various impacts that forest fires can have. These impacts, which are closely related, generally fall into three main categories: environmental, economic and human health [13].

Ecological effects

As stated previously, forest fires have both positive and negative effects.

Small, low-intensity fires or controlled burns can increase soil fertility by clearing out dead organic matter and releasing the nutrients it contains more quickly into the soil. Some plants require fire to reproduce, such as the lodgepole pine, whose cones need to be exposed to high temperatures to release their seeds [14]. It also has the ability to eliminate pests and diseased plants by burning them, preventing the spread of disease between trees. Another important aspect is the removal of fuel. In fact, small and controlled fires reduce the risk of devastating fires. This is even more important today, as climate change has created drier conditions and organic fuels are more likely to catch fire, creating a positive feedback loop as represented in Figure 1.2 [8][15][16].

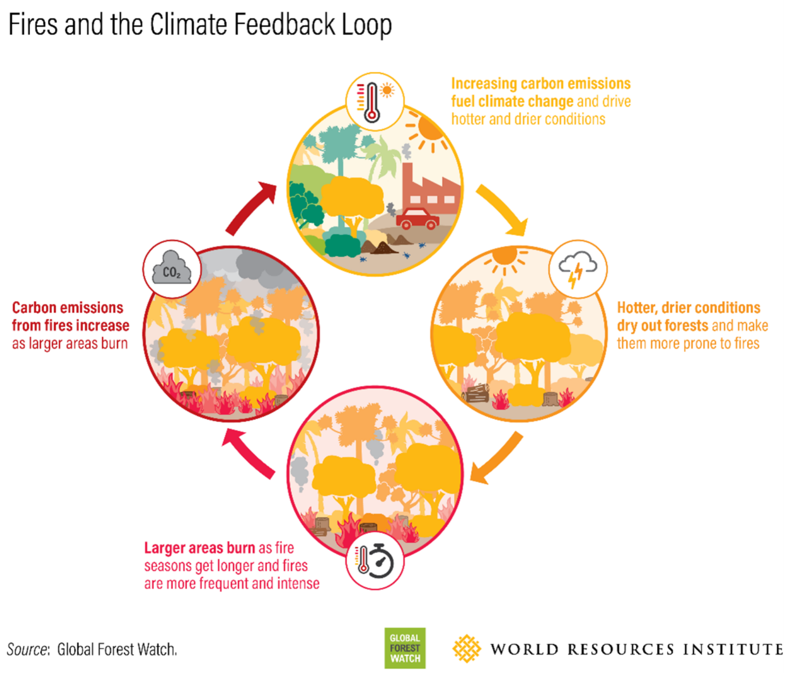

Figure 1.2: Dry conditions and the expansion of human activities into forested areas are important factors increasing the fire activity, from [8]

On the dimmer side, the major products of forest fires are carbon dioxide and water vapour. Evaluating the amount of CO_2 emitted by a fire is not an easy feat as these emissions are influenced by various interdependent factors, including forest fuel characteristics, burning efficiency, fire phase and type, meteorology, and geographical location [17][18]. With CO_2, the type of gases present in the smoke of a fire are CO, CH_4, NMVOC, NO_x, NH_3 and N_2O [12]. It also contains particulate matter (PM), divided in two categories: the coarse particles (PM_{10}), particles with diameters generally larger than 2.5 µm and smaller than or equal to 10 µm; and the fine particles ($PM_{2.5}$), particles with diameters smaller than 2.5 µm. The latter also includes the ultrafine particles, with diameters less than 0.1 µm [19].

The fuel characteristics and consumption may contribute to 30% of the uncertainties. The burning efficiency, ratio of carbon as CO_2 to total carbon in the fuel, varies with the vegetation type and its moisture content. The different fire phases, pre-ignition, flaming, smouldering and glowing, emit different proportion of gases. The type of fires burns differently. The heading fire, the fast spreading type, has high propagation speed and fuel consumption rate, and backing fire, the slow spreading type, has low propagation speed and long residence time. The former has a low burning efficiency and less oxidized emissions, and vice versa for the second [20].

Table 1.1: Average emissions released by wildfires in the Mediterranean biome, depending on the fuel type, from [21].

Fuel type	Average of emissions per burned hectare [Mg/ha]
Mediterranean long-needled conifer understory with shrubs	61.38
Tall Mediterranean shrublands and heathlands	55.42
Long broadleaved litter	49.45
Continuous tall Mediterranean grassland	46.21
Temperate and Alpine heathlands	17.21
Sparse and very short grassland	6.6

Table 1.2: Estimates of carbon emissions by wildfires in the Tundra biome, per area of forest (Mg C/ha) by vegetation cover types, from [22].

Fuel type	Estimates of carbon emissions per burned hectare [Mg C/ha]
Larch	15.5 – 18.8
Pine	16.7 – 18.0
Deciduous/mixed	13.7 – 17.5
Dark coniferous	12.7 – 20.4

Economic effects

Fighting wildfires is expensive. Over the last decade, the US Department of Agriculture's Forest Service and the Department of the Interior estimated that it cost more than $3 billion per year to suppress wildfires. And that number will not decrease with time, as they expect an increase ranging from 17% to 283% after 2050 [23]. But the direct costs of forest fires do not stop at suppressing them. From timber losses to property damage, passing by evacuation costs and death and injuries, their impacts are varied [4].

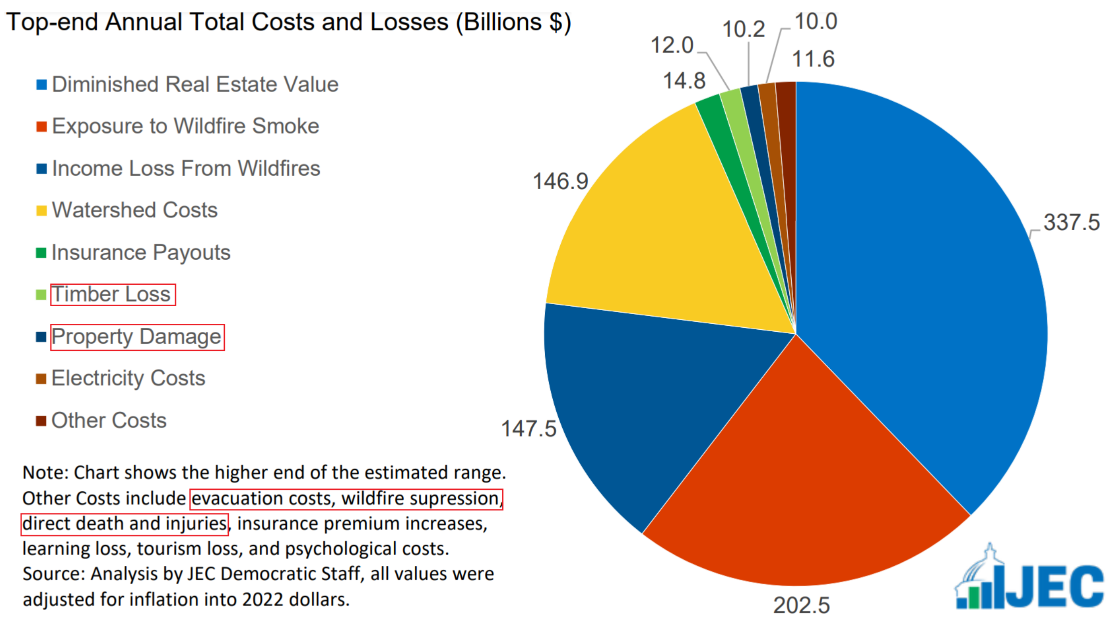

Figure 1.3: Wildfires cost up to $893 billion per year, in the USA. The read-boxed elements are directly related to wildfires, adapted from [4].

But wildfires have more subtle and impactful influence on the economy. In the western United States, they cause asset depreciation. People move away from areas at risk from fires and real estate values, in these regions, decrease, decreasing the possible tax base at the same time. The value from Figure 1.3 representing this cost is the total cost estimated and is expected to be realized in one to five years. That cost could be spread over the five years [4].

The costs of short- and long-term exposure to wildfire smoke are also very high in Figure 1.3. This includes all costs associated with hospital admissions for cardiovascular disease, respiratory disease and premature death [4]. In Canada, the economic impact of particulate matter from wildfires through hospital costs is estimated to range from $410 million to $1.8 billion per year for acute health effects and from $4.3 billion to $19 billion per year for chronic health effects [24].

Wildfires disrupt businesses, force evacuations, and hinder employees from getting to work. Because of this, they have an indirect impact on the national income. They are also a source of losses for insurance companies, which have to compensate their customers, whether for loss of money because a business has had to close, loss of property or the cost of evacuations [4].

Another effect the wildfires have is the pollution of water supplies. Such water needs to be treated, alternative supply needs to be found, and this comes with a certain cost, depending on the severity and volume of polluted water. There are also minor losses due to reduced tourist numbers in or close to high-risk regions and social costs [4]. Ultimately, the effects of forest fires on the economic aspect of the human world are many and varied.

Effects on human health

People can be injured by forest fires by inhaling smoke or being burnt by the flames [25].

The burns are more likely to affect the firefighters and rescue workers, and people living near wildfires [26].

The effects of the smoke cover a wider area than the flames. Wildfire smoke is a mixture of air pollutants, of which PM is the principal human health threat. $PM_{2.5}$ is associated with premature death and can cause or aggravate diseases of the lungs, heart, brain/nerve system, skin, intestines, kidneys, eyes, nose, and liver [25][27]. In Canada, the annual health effects of $PM_{2.5}$ from wildfire are estimated to be 54 to 240 premature deaths due to acute exposure and 570 to 2,500 premature deaths due to chronic exposure [28].

It also causes mental illness due to mental stress resulting from economic loss, casualties and forced evacuations [29].

Certain groups are more vulnerable to the health effects of wildfire smoke, including children, the elderly, pregnant women or those with chronic illnesses [26].

1.2 Forest Monitoring

Forest monitoring is essential to control and suppress forest fires. Sensors used in remote sensing can have multiple form but also multiple platforms on which they can be mounted. There are three categories: spaceborne, with satellites, airborne, with planes or UAV, and ground-based, with IoT devices, scanners, and plenty more [30].

Many techniques are in use today to monitor the evolution of the condition of a forest, a few of them will be described in this section. This is a non-exhaustive list.

Moderate Resolution Imaging Spectroradiometer (MODIS)

The Moderate Resolution Imaging Spectroradiometer is a satellite-based sensor. It orbits at an altitude of 705 km with an inclination of 98 deg°ever since December 18, 1999. It has multiple functionality due to its large range and its live coverage of the earth. It uses imagery to collect data and sends it at different rates, from daily, for short-term observation, to yearly for long term data analysis [31][32].

MODIS can be used in fire prevention, detection, and analysis.

Light Detection and Ranging (LiDAR)

LiDAR is a system that uses laser to detect objects. It emits short laser pulses at very high frequencies and measures the time-of-flight and intensity between the emission and reception of the pulse. It can be used to characterize forest fuels and prevent massive outburst of fires [30].

UAV Mapping

This technology can be paired with multiple sensors. Its purpose will be to fly over a forest, with a LiDAR, an infra-red camera, or other remote sensing technologies, and can provide real-time high-resolution data to help monitor wildfire activities. [33].

Wireless Sensor Networks for Fire Detection

Wireless sensor networks rely on the use of IoT devices. They are deployed in the forest, giving real-time data, which will depend on the sensor they are equipped with, and do not require supervising to alert in case of fire hazard [5].

The latter is the technology of interest in this thesis. Its complex

1.3 IoT Node Architecture

This thesis specifically targets IoT sensor networks. Although its primary focus is not on the design of IoT nodes, understanding their architecture is important. An IoT node is composed of several key modules, each with a specific function, as illustrated in Figure 1.4.

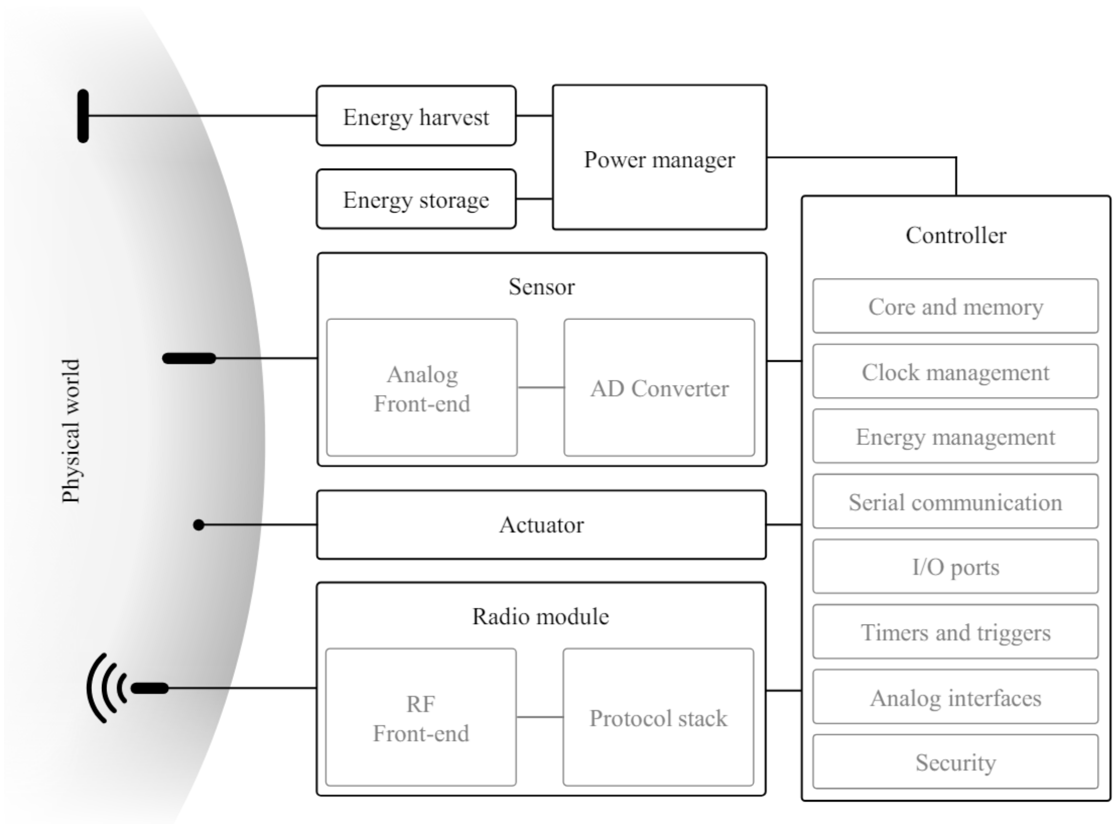

Figure 1.4: Generalized architecture of an IoT node used for remote sensing, from [34]

These modules include:

Processing

The central component of an IoT node is the Microcontroller Unit (MCU). It is responsible for executing the node's firmware, processing sensor data, and managing communication with other modules. The functionality of the MCU is critical for the overall performance and efficiency of the node [34][35].

Transport

An IoT node can communicate with other IoT nodes, servers or other devices. The transmission of data by IoT nodes can be achieved via multiple communication methods. These encompass wireless protocols such as Wi-Fi, Bluetooth, and LoRa. Each communication technique has its own advantages and trade-offs, and understanding them is crucial to deploy effective IoT networks [36].

Perception

Depending on the application, an IoT node will have different ways to connect with the physical world. The perception module is the one performing that task. It can be equipped with various sensors to gather environmental data. Typical information collected include temperature, carbon dioxide, humidity, and pressure [34][37].

Power management

The power management unit (PMU) is an essential component of the IoT node, as it manages the power consumption of the node and regulates the power supply to different components according to their needs. In low power nodes, this module optimises power consumption and ensures that each component operates within power constraints. [34].

Energy source

IoT nodes can be powered by various energy sources. A non-exhaustive list of these sources includes batteries, solar harvesting systems, and recharging mechanisms using an Unmanned Aerial Vehicle (UAV). The energy source will depend on the context in which an IoT node is used. In remote applications, the most commonly used solution is batteries [38].

1.4 Long Range Wide Area Network

In remote-sensing application, the combination of low-power consumption nodes and long-range communication constrains a designer to the use of Long Range Wide Area Network (LoRaWAN), a protocol designed for wireless communication in IoT applications. [34] This section provides an analysis of its operational process.

As displayed on the Figure 1.5, a LoRaWAN enables long-range communications for low-power devices. The network has three components, the low-power node, the relay node, or gateway, and finally the cloud or server. The sensor is low-power and therefore can only send packets to a certain distance. The gateway is deployed in said range to relay the information the low-power node sent.[34]

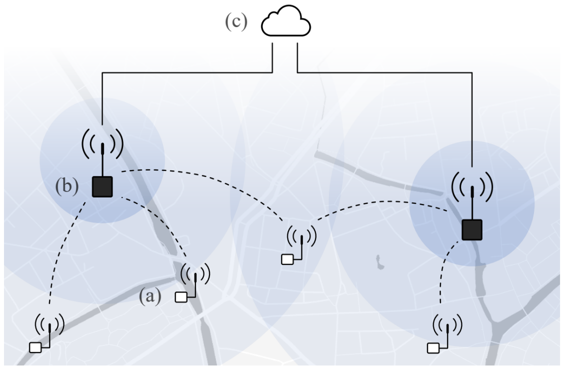

Figure 1.5: The IoT nodes (a) communicate with one of more gateways or base stations (b) via long-range connectivity. The gateways then communicate with a server or the cloud (c) where data can be visualized and interpreted, from [34].

1.5 Energy Sources

In light of the information presented in the previous section, it is evident that an IoT node deployed in a forest setting, or any remote sensing application, cannot be powered by a cable connected to the grid. This section will explore alternative energy sources available to an IoT node, including an analysis of their production process, their operating process and the global trends concerning them.

Solar-energy harvesting

Solar-harvesting technology employs photovoltaic (PV) cells to convert sunlight into electricity. There are a number of different technologies available for this purpose, including amorphous silicon, cadmium telluride, copper indium gallium selenide, and crystalline silicon. Among these technologies, crystalline silicon is the most prevalent, with monocrystalline silicon (mono-Si) emerging as the dominant technology within the category due to its high efficiency and longevity [39]. The production of electricity in a solar cell is based on the photoelectric effect, where the energy contained in the photons from sunlight energises electrons from atoms in the silicon, their movement within the cell resulting in the generation of an electric current [40].

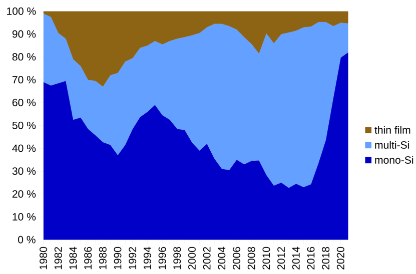

Figure 1.6: Global photovoltaics market share by technology, from 1980 to 2021 [39].

As shown on the Figure 1.7, a mono-Si solar cell goes through multiple steps to go from silicon to the finished product [41]. The silicon is melted and crystallised into a single-crystal ingot using the Czochralski process [42]. The ingot is then cut into thin wafers. After texturing to reduce reflection losses and cleaning with acid to remove any particles from the surface after texturing, the wafers are doped to increase efficiency. They are then subjected to a series of processes to protect the cell and undergo rigorous testing to ensure their functionality. Finally, the cells are assembled into modules for future deployment [43].

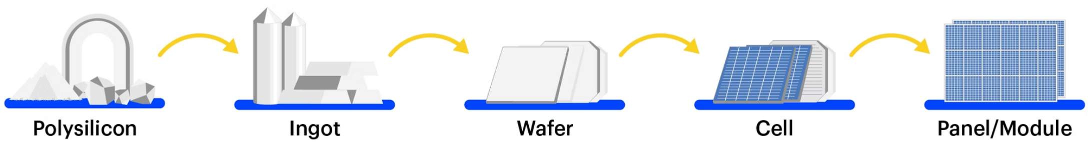

Figure 1.7: Key stages in the manufacturing of solar PV, from [41].

As of today, mono-Si dominates the global market, followed by poly-Si and thin film, with the proportion represented on Figure 1.6 [39]. The largest producer of mono-Si is China, with around 80% of the global manufacturing in ll the manufacturing stages of solar panels [41].

Battery power

One of the most widely used energy storage, the battery exists in multiple size, forms and chemical composition. These device stores energy in a chemical form and releases it as electricity within a closed system. To achieve this, its relies on an electrochemical reaction between two electrodes, called cathode and anode. This reaction is dependent on the composition of the electrodes. Therefore, the choice of material for the composition of a battery is essential. It also determines the type of battery, i.e., rechargeable or non-rechargeable [44].

The composition of a battery will also determine the rest of its caracteristics, such as its capacity, which determines the total amount of energy it can store, and its energy density, energy stored per unit volume or weight. Other critical factors include the, cycle life (number of charge/discharge cycles it can undergo before significant degradation), and charging time [44][45].

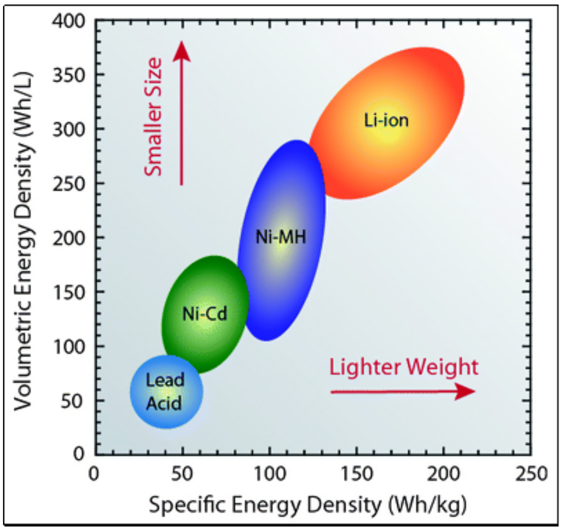

Figure 1.8: Battery Energy densities, from [46]

This Figure 1.8 highlights the superior energy density of lithium-ion batteries Their production involves several key steps: First, the materials for the cathode, anode, and electrolyte are prepared. These materials are then processed to form the electrodes, which are assembled into cells. The cells undergo a formation process, which involves initial charging to stabilize the battery's internal structure. Finally, rigorous testing ensures that each battery meets the required performance and safety standards [44][47].

The production of Li-ion batteries involves the extraction and processing of various materials, depending on their chemical compocision. These materials are extracted through mining operations, with lithium sourced from salt flats or spodumene ores, cobalt primarily from the Democratic Republic of Congo, and nickel from laterite or sulfide deposits [47].

Unmanned Aerial Vehicle Recharged

This energy source is a new alternative to supplying techniques, still at the state of prototype [48].

Figure 1.9: UAV approach to extend the lifetime of IoT devices in different use-cases [48].

The Unmanned Aerial Vehicle (UAV) recharged solution relies on the Wireless Power Transfer technique. This method involves transmitting power wirelessly over a distance using electromagnetic fields. It allows the UAV to recharge IoT nodes without physical contact [49].

The way it is applied in this context is as shown on the Figure 1.10. The IoT node has a receiver (RX) coil and a rechargeable battery. The UAV carries the transmitter (TX) coil and multiple batteries to carry the power that needs to be transferred to the node. It then hovers or land on a platform below the device and the WPT takes place, recharging the battery of the IoT node [48].

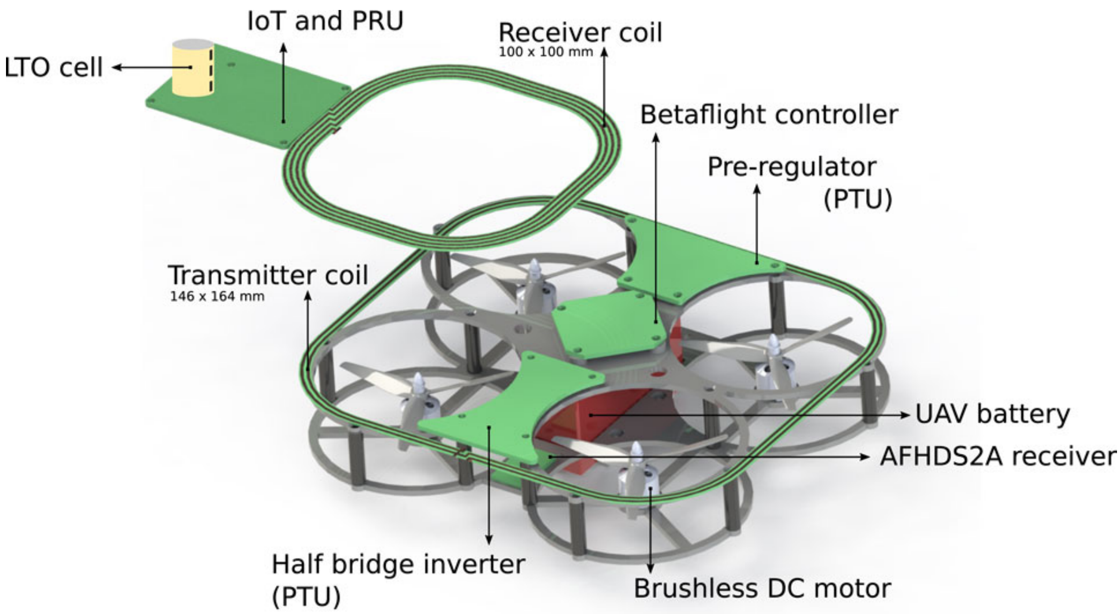

Figure 1.10: UAV prototype, from [48].

In summary, the UAV solution offers a promising method for extending the operational life of IoT nodes, particularly in remote or hard-to-reach areas, by autonomously delivering energy or replacing batteries, thereby reducing the need for frequent human maintenance [48].

Its production process is similar to that of a UAV, but needs to be modified to have the implementation of the TX coil in its structure.

Chapter 2

Related Work: LCA of IoT Nodes in Forest Monitoring

The previous chapter gave an overview of the problem that the application is trying to solve. This chapter reviews previous work on IoT nodes used for forest monitoring, both in terms of LCA and node design.

Van Mulders et al., 2024

A recent study by *Van Mulders et al. (2024)* [48]. In this paper, the environmental impact of two IoT systems, used for environmental monitoring, was considered, one low-power and one with medium power consumption. An operation time of around 2 months was chosen to dimension the LTO batteries. The first IoT device consumes 10 [J/d] and requires a battery with a capacity of 0.144 [Wh] (60 mAh at 2.4 V), and the UAV hovers over the device to perform the WPT. The second device consumes 200 [J/d] and its battery is bigger, with a capacity of 3.12 [Wh] (1.3Ah at 2.4V). The UAV is unable to charge the battery fast enough to hover, a landing alternative is used to be able to transfer the full amount of energy.

In addition to the battery, the flows considered are the IoT manufacturing with the additional WPT hardware, and the UAV production. For the UAV, a lifetime of 400 hours is modelled, with the battery degradation and replacements. The LCIA results obtained with the ReCiPe 2016 midpoint (H) for each device and its battery are shown in the Figure 2.1.

To contextualise the results, the author compared the two devices, separately, with a typical IoT device, with three servicing methods: full device replacement after 1 year; battery replacement, and full device replacement after 5 years. The results of the comparison are displayed in Figure 2.2.

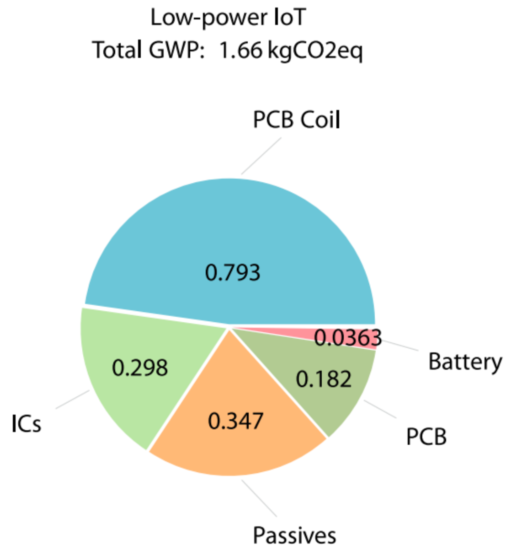

Figure 2.1: LCIA results of different parts of the IoT node for the GWP [kgCO_2eq.] for the two IoT devices, from [48].

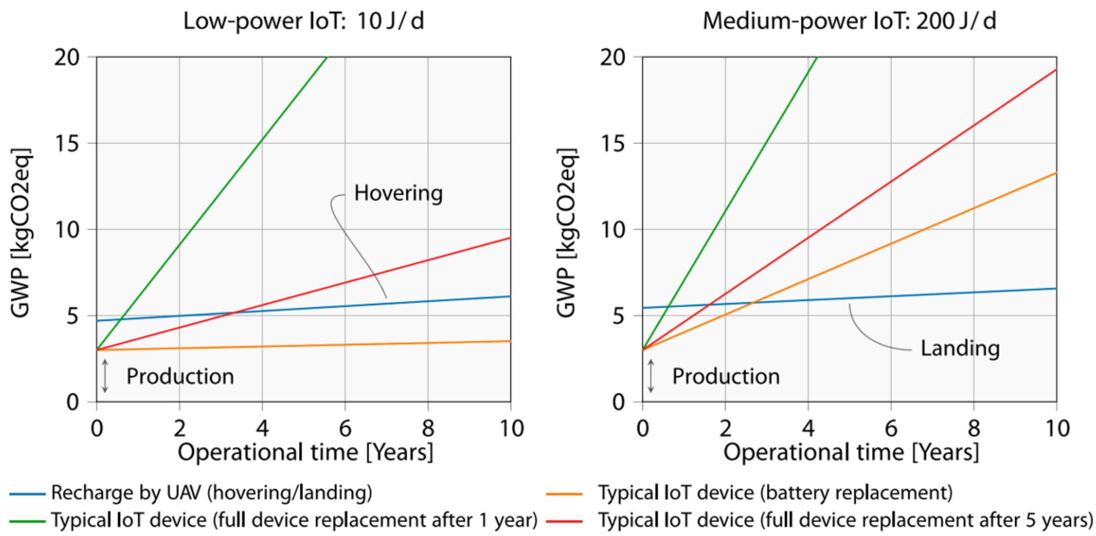

Figure 2.2: Comparison in average environmental impact of low- and medium-powered UAV devices with different servicing methods, from [48].

The study indicates that the UAV recharging approach can enhance the longevity of remote IoT nodes while reducing the ecological footprint for devices with medium to larger power needs.

Maistriaux et al., 2022

A recent study by *Maistriaux et al. (2022)* [50]. The purpose of it is to develop a comprehensive open-source parametric model of battery-powered IoT nodes use phase in environmental monitoring applications. To demonstrate the use of the model as an eco-design, the study applies it to a forest monitoring case study.

The flow representing the IoT node is a prototype and its details are as follows : An ultra-low power MCU, *Apollo3 Blue*, is combined with the sensor *BME680* from *Bosch*, the radio module *RFM95*, the PMU *XC6206* on a 4-layer PCB, in a casing made of ABS plastic, aluminium, and steel. The prototype is powered by three *Alkaline AAA batteries* of 2800 mAh each.

The power consumption model is based on the datasheet of each component, displayed in the left picture of Figure 2.3. The model was validated experimentally, and the values for the characterization are shown in the left picture of Figure 2.3. The LCIA results for the cradle-to-gate of the prototype and its batteries are displayed in the Figure 2.4

	Module state	**Measure**	**Datasheet**	**Characterization**
MCU	Sleep	I_{sleep}	3.2 μA	2.7 μA
	Active @48MHz	I_{active}	494 μA	573 μA
	SPI	T_{SPI}	- ms	306 ms
	I^2C	T_{I^2C}	- ms	106 ms
	FWI calc.	T_{FWI}	- ms	1.5 ms
Sensor	Sleep	I_{sleep}	0.15 μA	32.8† μA
	TPHG ††	I_{TPHG}	90 μA	78.2 μA
Radio	Sleep	I_{sleep}	0.2 μ A	0.6 μA
	RX	I_{RX}	11.5 mA	11.3 mA
	TX @+17*dBm*	I_{TX}	87 mA	86.23 mA
	TX @+20*dBm*	I_{TX}	120 mA	119.05 mA

† BME680 EVB sleep power significantly differs from BME680 datasheet. Characterization value was therefore used to validate the power consumption model.
†† Average current when sensor measurements are performed at 5 minutes interval.

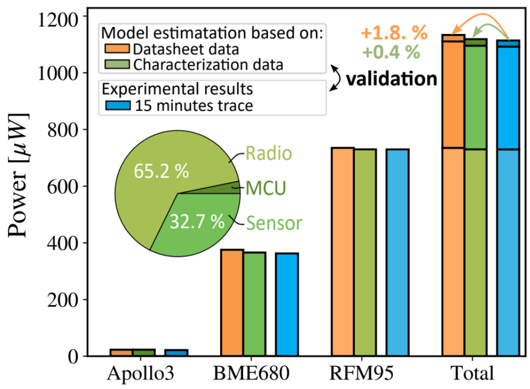

Figure 2.3: Left : Operating electrical characteristics of the three modules of the prototype, at 3.3V [50]. Right: Validation of the power consumption model based on the prototype, with a LoRa payload of 50 bytes, a sensing every 5 min and a transmission every 15 min [50].

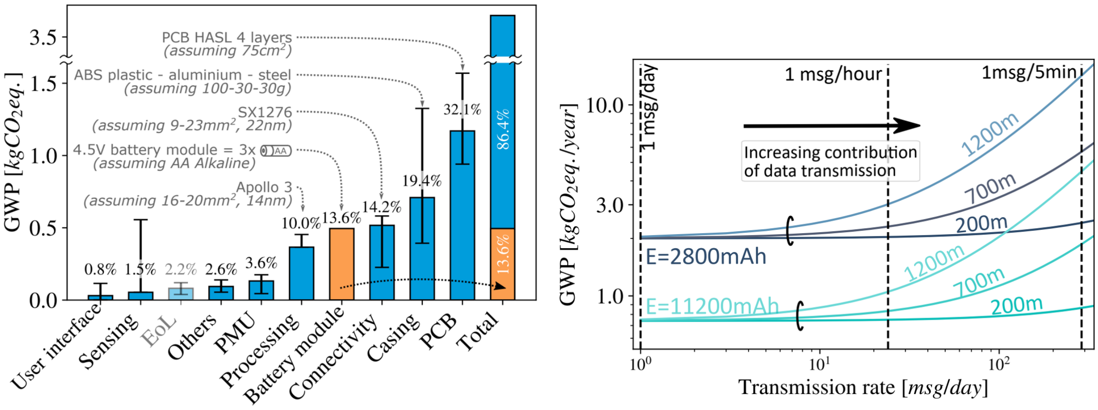

Figure 2.4: Left: Breakdown of the cradle-to-gate LCIA results for the prototype. The total is 3.65 [kgCO_2eq.][50]. Right : Impact of transmission rate, node-base station distance and battery capacity on GWP [50].

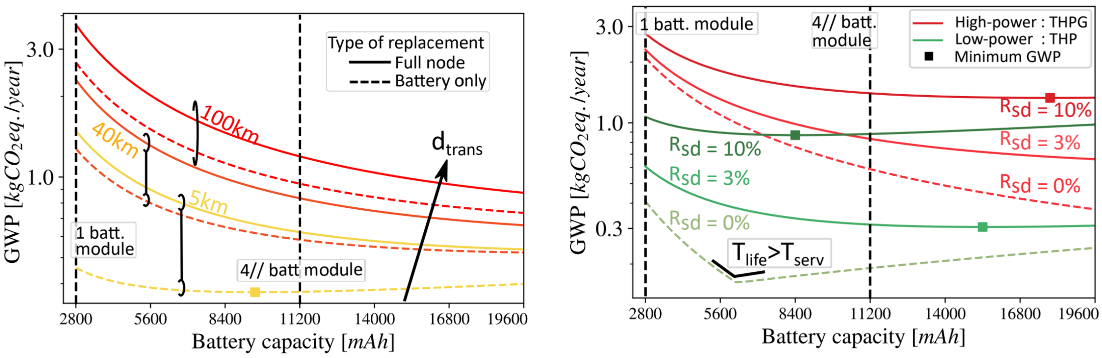

Figure 2.5: Left: GWP with respect to battery capacity for transport distances of 5, 40 and 100 km [50]. Right : GWP with respect to battery capacity for two types of sensing and three self-discharge rates R_{sd} [50].

To estimate the service lifetime, three key parameters were considered, the transmission rate, the node-base station distances and the self-discharge rate. Their influence on the carbon footprint is shown in Figure 2.5.

This study highlights that often overlooked parameters can represent serious hotspots, both in the design and the use phase.

Chapter 3

Life-Cycle Assessment of a Sensor

The purpose of this chapter is to develop the Life-Cycle Assessment (LCA) methodology that allows the comparison between different supply strategies for forest-monitoring IoT sensor networks. After the goal and scope definition, the inventory analysis and the LCI model are explained in detail. The results of the LCIA are analysed from a multi-indicator perspective.

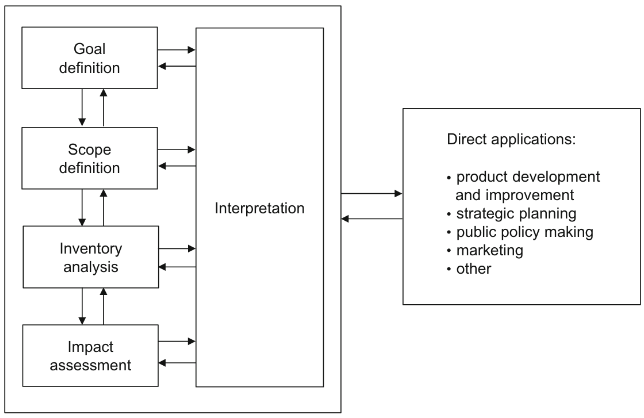

Figure 3.1: Framework of LCA modified from the ISO 14040 standard from [51]

Each section of this chapter will begin with a brief introduction presenting the theoretical framework derived from M.Z. Hauschild's "Life Cycle Assessment" [51]. Using this established methodology systematically facilitates the assessment of environmental impacts of products or processes across their entire life-cycle, ranging from resource extraction through to disposal. By defining clear goals and scope, conducting thorough life-cycle inventories, assessing impacts comprehensively, and interpreting findings thoughtfully, LCA provides a robust framework for understanding and mitigating environmental footprints associated with various industrial and consumer activities.

It should be noted from Figure 3.1 that an LCA is an iterative process and that the LCA practitioner will often have to revise his work several times.

3.1 Goal and Scope Definition

The goal and scope definition are two separate steps in the LCA methodology but are close in function as both are used to set the boundaries and context of the LCA. Furthermore, the former is the basis of the latter and both are very important to consider when interpreting the results of the study because they have a strong influence on the validity of the conclusions, therefore they will be grouped in this section. The results of an LCA are dependent on the goal and scope of the study.

Goal Definition

The ***goal definition*** is the first phase in an LCA. During that phase, it is required of the LCA practitioner to explain the intended applications of the results in order to create a decision context and explain the reasons for carrying out the study, while showing the limitations due to the methodological choices. It should also be the section in which the writer describes the target audience of the study. The penultimate step is to display whether the LCA study will be of a comparative nature and if it is intended to be disclosed to the public. And finally, the writer must clearly identify who the commissioner of the study is and any other influential actors.

In this study, the ***goal*** is to evaluate the improvement potentials of product design through the comparative assertion of the environmental impacts associated with the power source of an IoT node used in forest monitoring. Three different energy sources will be compared:

- **Solution 1:** Solar-energy harvesting with a **photovoltaic cell**, referred to as **Solar solution** for the rest of the thesis,
- **Solution 2: Non-rechargeable batteries**, referred to as **Battery solution,**
- **Solution 3: Rechargeable batteries** recharged every two months by an unmanned aerial vehicle (UAV), referred to as **UAV solution**.

Each solution will be developed in depth in section 3.2.

It will be a micro-level decision-support LCA, as it has no impact on the background processes, of comparative nature and public. The influential actors of this LCA are the research teams of Professor David Bol from UCLouvain and of Professor Liesbet Van der Perre from KU Leuven, and Dryad Networks GmbH (Dryad), whose influence will be explored in greater depth later in this thesis. The target audience of this study are research teams working on sensors and IoT nodes producers.

Scope Definition

The **scope definition** phase of LCA establishes the foundation for the entire study by defining the product systems to be assessed and outlining how the assessment should be conducted. This phase ensures that the methods, assumptions, and data used are consistent, which is critical for the reproducibility of the study. The main components of scope definition include [51][52]:

Product systems to be studied:

Identifying which product systems will be evaluated is the first step. This involves specifying the products, processes, or services under examination and their life-cycle stages.

Functions of the product system:

Clearly defining the functions that the product system performs is essential. This helps in understanding the purpose of the product and its role in fulfilling certain needs or requirements.

Functional unit and reference flow:

The functional unit quantifies the performance of the product system, serving as a reference to which all inputs and outputs are normalized. The reference flow is the amount of product necessary to fulfil the functional unit.

System Boundaries:

Establishing system boundaries delineates which processes and stages of the life-cycle are included in the study. This could range from cradle-to-grave (full life-cycle) to cradle-to-gate (from raw material extraction to manufacturing) assessments.

Impact categories and LCIA method:

Selecting relevant impact categories (e.g., global warming potential, water use) and choosing an appropriate Life-Cycle Impact Assessment (LCIA) method are crucial for evaluating the environmental impacts.

Assumptions and limitations:

Documenting the assumptions made during the study and acknowledging its limitations are important for transparency and credibility.

Product system considered

The product system is a subsystem of a large-scale remote sensing system, comprising sensors, excluding the gateways and cloud platform of the whole system. The modules are considered to be installed in Southern Europe, in this study case in the "Parc de la Sainte-Baume", France. Three scenarios are appraised, each one employing an alternative energy source. The three energy source variants are described in subsection 3.2.2.

The base case is the Solar solution. A partnership has been organised with Dryad to provide a full LCA of their product in exchange for their Bill of Materials (BoM) for the Wildfire sensor. The BoM is under strict Non-Disclosure Agreement (NDA), all information on the Wildfire sensor in the following pages of this manuscript is public information available on Dryad's website [5]. Table 3.1 describes the characteristics of the product system for the base case, the Solar solution, i.e., the technical data of the Wildfire sensor.

Table 3.1: Key parameters of the product system — base case.

Parameter	Assumption	Note
Sensing range	80-100 m	From [53]
Sensor per ha ratio	0.7 in high-risk area 0.1 in low-risk area	From [53]
Communication range	1 km	Dryad's documentation
Size	3.0 x 3.0 x 0.93 mm.	Bosch BME688 datasheet [54]
Gas sensor Sensors	CO, CO_2, H_2, VOC, Temperature, Humidity, Air Pressure.	
Installation location	"Parc naturel régional de la Sainte-Baume" France	
Support	Mounted on a tree at a 3m height	From [53]

As this LCA is of a comparative nature, some parameters will vary with the solution observed.

Table 3.2: Key parameters different for each solution.

Parameter	Solar solution	Battery solution	UAV solution
Power source	Solar-powered	Battery-powered	Battery-powered
Energy storage	Supercapacitor (SC)	Non-rechargeable battery	Rechargeable battery
Weight	136g	286g	122g
Size of casing[1]	19 x 9,2 x 1,2 cm	19 x 9,2 x 4.4 cm [2]	19 x 9,2 x 3 cm [3] + 8 x 8 x 3 cm
Lifetime	10 – 15 years	10 years	10 years

[1] Only the height varies according to the size of the battery cells used.
[2] The battery is ⌀3,2 x 6,1 cm.
[3] The battery is ⌀1,8 x 6,5 cm and the UAV solution requires a landing platform for the UAV, assumed to be made of the same material as the rest of the casing.

Functional unit

The functional unit is defined as the coverage of the forest along 1 km of road in a Mediterranean environment, for 10 years with 0.7 sensors per ha in the area between 0 and 1 km from the road and 0.1 sensors per ha in the area between 1 and 2 km by the large-scale remote sensing subsystem, as represented on the Figure 3.2.

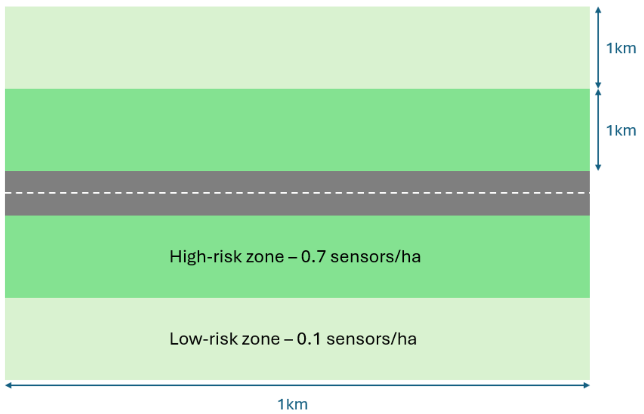

Figure 3.2: Visual representation of the functional unit. The risk of fire is greater close to roads, as forest fires are often started by humans [10]. Hence the high-risk zone close to the road and the low-risk zone further away.

Reference flow

The reference flow is a sensor powered by a power unit, capable of sensing the environmental properties of its surroundings continuously.
For Solar solution: 1 IoT node powered by a solar panel.
For Battery solution: 1 IoT node powered by a non-rechargeable battery.
For UAV solution: 1 IoT node powered by a rechargeable battery and the fraction of a UAV, as it is shared among 132.5 nodes.

System boundaries

This is a cradle-to-grave analysis, excluding the end-of-life (EoL). This means that almost all significant life-cycle stages relative to the studied product were considered, from raw-material extraction, through processing and production, to distribution and use. The choice to exclude the EoL from the scope was based on the information that processing of electronics has a rather small environmental impact compared to the total picture, [55], and the modelling of these EoL scenarios is lacking in LCA databases.

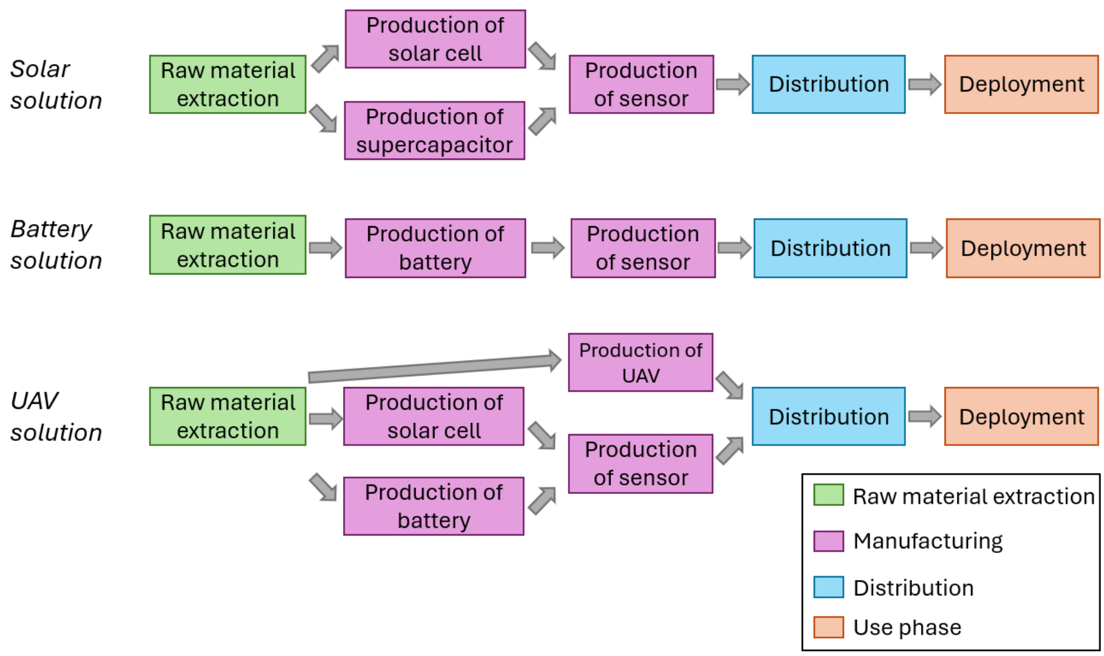

Figure 3.3: System boundaries diagram for the hardware composition of each solution considered in the functional unit, inspired from [51].

- **Raw-material extraction:** This includes the extraction and pre-processing of the raw materials needed to manufacture the sensor components. It also includes the transport of raw and pre-processed components between each step of this process.

- **Manufacturing:** This accounts for the energy and material flows required to manufacture the sensor. It also includes the transport of materials between the extraction site and the treatment site to manufacture and any transport required between component manufacture and module assembly. The equipment required for the use phase is excluded, with the exception of the UAV, the production of which is included in the manufacturing process.

- **Distribution:** This covers the distribution of finished sensors to the installation in Southern Europe. The distribution of finished UAVs is included in the UAV solution.

- **Use phase:** This involves the deployment of the sensors in the forest and any maintenance required, as well as the production of the car used. For the UAV solution, it includes the power generation required to fly the UAV and recharge the batteries, as well as the energy required to bring the UAV within range of the sensors.

Modelling and calculations

The LCA model is built in GaBi software, using the GaBi database to model most of the flows. The exceptions are the solar cell, the supercapacitor (SC) and the two types of batteries, as they are not represented in the database. They are therefore modelled using LCA results from scientific research.

LCIA method

For most impact categories, the International Reference Life Cycle Data (ILCD) Environmental Footprint 3.0 (EF 3.0) will be used as the LCIA method for calculating impacts. The only exception is the metal and fossil resource scarcity categories for the solar solution, for which the ReCiPe 2016 midpoint (H) method will be used to calculate the results. The UAV and Battery solutions are using EF 3.0 for said categories.

Impact categories

The impact categories selected to compare future LCIA results are as follows:

- Climate change;

- Ozone depletion;

- Human toxicity, non-cancer effects;
- Human toxicity, cancer effects;
- Photochemical ozone formation;
- Acidification;
- Terrestrial eutrophication;
- Freshwater eutrophication;
- Marine eutrophication;
- Freshwater ecotoxicity;
- Water resource depletion.

Due to the differing calculations methods, as explained in the previous point, the metal resource scarcity and fossil resource scarcity categories will be evaluated for the Solar solution but used as for the comparison. For the other two solutions, there is no information regarding the fossil resource scarcity, but the meta resource scarcity will be used to compare the two.
Three other categories can be evaluated with the EF 3.0, the land use, the ionizing radiation, human health, and the particulate matter emissions. They are not considered here. On one hand, because the version used in the reference for the Solar solution uses an older version of EF 3.0, which as a different reference for the particulate matter emissions. On the other hand, because that same reference does not evaluate the impacts for the land use and the ionizing radiation.

Assumptions

The thesis clearly describes and explains when primary data are not available and estimates or assumptions have been used.

Limitations

The main limitation of this study is the lack of datasets on the solar panels, lithium battery and SCs in GaBi's database. This causes discontinuity in the sources.

Normalisation and weighting of the results are not employed in this study.

3.2 Inventory Analysis

The Life-Cycle Inventory (LCI) is the third and most intricate step of an LCA. During this phase, the LCI model is created. Its function is to collect and compile all the processes in the studied product system under consideration that enter, move within or leave the system boundaries, as theoretically represented in Figure 3.4. It is guided by the goal and scope definition.

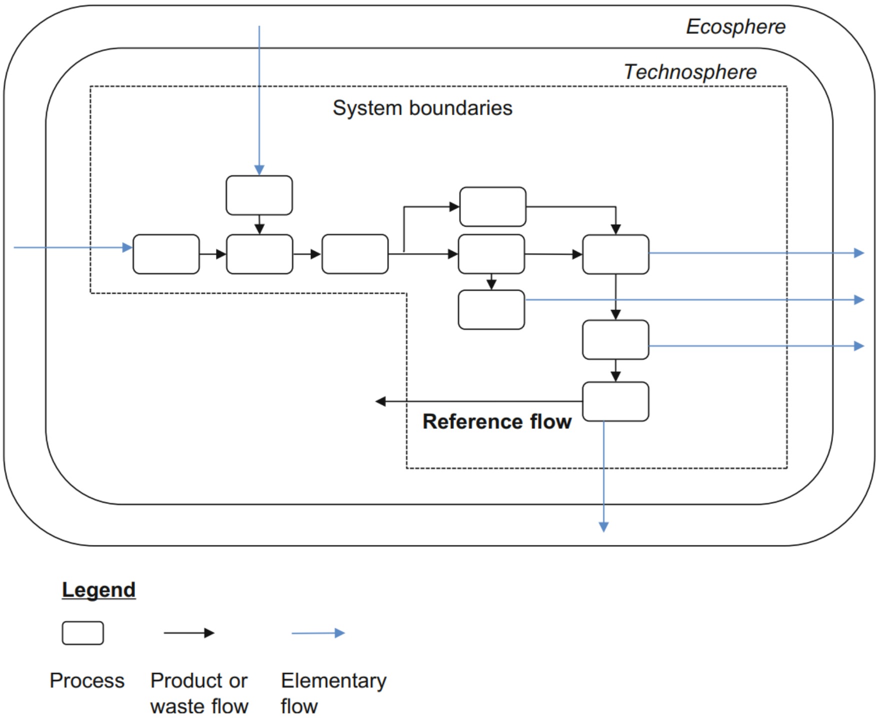

Figure 3.4: Example of the system boundaries, from [51]. The LCI models all processes and flows in and entering the boundaries.

During the LCI analysis phase of an LCA the collection of data and the modelling of the flows to, from and within the product system(s) is done.

The LCI analysis has six main function: identify the processes for the LCI model of the product system; plan and collect the data; construct and check the quality of unit processes; construct the LCI model and results; prepare the basis for uncertainty management and sensitivity analysis; and report the results.

The LCI of this thesis is divided into four sections:

- The sensor production: covers all non-solution specific processes, without going in too many details;

- The three energy sources: explains the construction of the solution specific processes in a detailed way;
- The distribution;
- The use phase.

The BoM is acquired from Dryad's BoM for their Wildfire sensor [5] which is placed under strict NDA and will not be displayed in this work. The UAV model is based on the works from PhD candidate from KULeuven [34][56].

3.2.1 Sensor Production

Table 3.3: BoM of the studied case, inspired by the Silvanet Wildfire Sensor. Detailed names of the components used are not shown due to NDA.

Component		Quantity	Scaling factor based on	Source
Microcontroller		1	Die area	GaBi 2023.1 database [57]
Gas sensor		1	Die area	
DC-to-DC converter		1	Die area	
Flash memory		1	Die area	
Coil		2	Mass	
Capacitors		4	Capacitance	
Resistor		9	Resistance	
Quartz		1	Mass	
Antenna		1	Mass	
PCB		1	Area	
Protective vent		1	Mass	
Casing		1	Mass	
Energy storage	Solar solution	2	Capacitance	Cossutta et al. [58]
	Battery solution	2	Mass	Eracka et al.[59]
	UAV solution	1	Mass	Eracka et al.[59]
Energy source	Solar solution	1	Area	Galley et al. [60]
	Battery solution	N/A	N/A	N/A
	UAV solution	1	Hours of flight	Van Mulders et al. [56]

Microcontroller Unit (MCU)

The MCU used in this case study is a wireless microcontrollers, meaning that it serves both the purpose of communication and processing. It uses the 868 MHz ISM frequency band.

Gas sensor

The gas sensor has no existing process in GaBi's database but will be modelised as a microphone, as their integrated circuit (IC) is similar.
Note to the reader: the gas sensor is always referred to as such to avoid confusion with the reference flow, i.e., the sensor.

Printed Circuit Board (PCB)

A two-layer PCB is used for this model.

For the Solar solution, the surface area of the PCB was provided by Dryad and will not be shared due to the NDA. For the other two solutions, the surface area was defined on the basis of the following assumptions: the PCB is covered at 15% with electronic components; both sides are covered; the total surface area occupied by the components is 157.5 [mm^2], data taken from the datasheet of the components used by Dryad; the batteries are not included in the surface area calculation.

This gives a total value of 524.95 [mm^2] of PCB for the two solutions. For the UAV solution, an additional area of 2483.88 [mm^2] must be added for the receiver coil, bringing the total PCB area for this solution to 3008.83 [mm^2]. The LCIA results will be separated, with the PCB for the RX coil associated with the energy source and the PCB for the components associated with the sensor production.

Protective vent

The purpose of the protective vent is to cover the opening in the casing to prevent water infiltration while allowing gases to enter. The vent is made up of two components, a polyester resin disc and a silicone sealant ring, the first acting as a protective cover, the second as a seal connecting the casing to the disc.

Antenna

The antenna is made from a tinned copper wire. After some research it was found that the proportion of tin to copper is negligible, less than 3% of the total mass of a wire for the greatest thickness of tin coating (20 µm) [61]. Therefore, the antenna is assumed to be all copper.

Table 3.4: Mass of material in a ⌀2 mm tinned copper wire.

	Cu	Sn
Density [g/cm^3]	8.935 [1]	7.289 [2]
Volume [cm^3]	0.458	9.1×10^{-4} to 0.0185 [3]
Mass [g]	4.09	6.63×10^{-3} to 0.135 [3]

[1] From [62].
[2] From [63]
[3] Min and max coating thickness from 1 to 20 µm [61].

Casing

The casing is produced directly by Dryad, with the help of injection moulding. The process requires plastic granulates and electricity and has an existing flow in the GaBi database. It is a manufacturing process with very few wasted material [64].

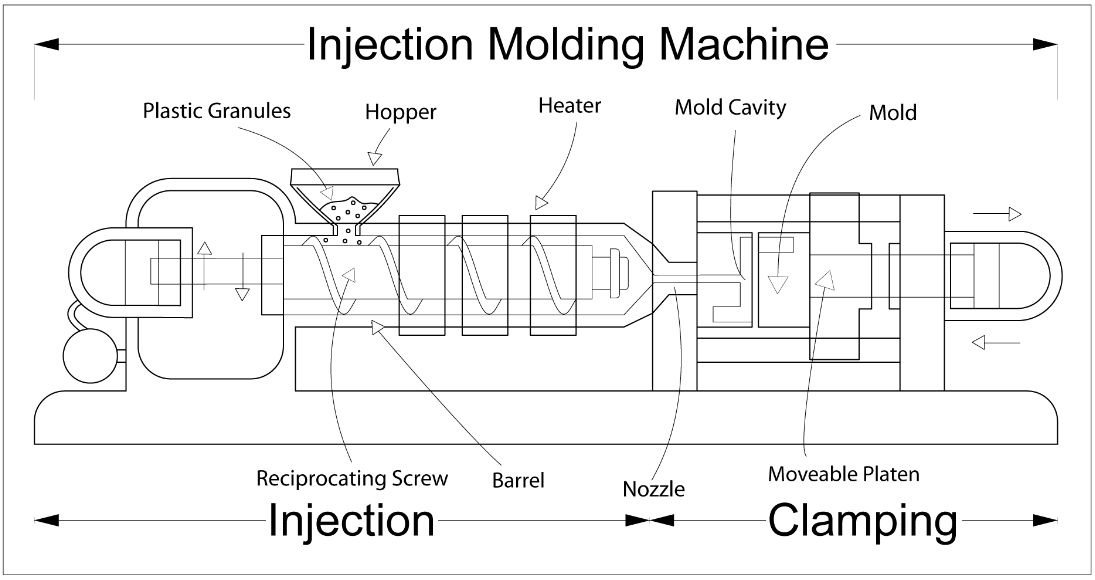

Figure 3.5: Injection moulding machine from [64]. The plastic granules enter the machine through the hopper. Then they are pushed towards the nozzle by the reciprocating screw while being heated to their melting point. At the nozzle, the plastic is injected in a mould, where it takes its intended form, to then be cooled [65]. It is a common manufacturing process for plastic parts.

The reference for the comparison is the Solar solution, as technical data were provided by Dryad.

Table 3.5: Differences between the casing of each solution and their scaling to the reference.

Parameter	Solar solution	Battery solution	UAV solution
Size	19 x 9,2 x 1,2 cm	19 x 9,2 x 4.4 cm	19 x 9,2 x 3 cm + 8 x 8 x 3 cm
Volume of plastic [cm^3] [1]	85.25	312.57	213.12
Scaling	1	3.67	4.43

[1] The volume is measured using SolidWorks software [66].

3.2.2 Three Energy Sources

Solar solution

The energy source for the Solar solution consists of two flows, the solar cell and the SCs. As the majority of solar cells produced in 2021 are made of monocrystalline silicon (mono-Si) [67], the solar cell flow will be represented by that technology.

A major issue arose when it came to assessing the impact of solar cells and SCs. At the time of writing, there are no solar cells or solar panels nor SCs in the GaBi database. To fill this gap, a literature review was carried out of papers that correctly applied LCA methodology.

Multiple LCA exist for solar modules. Most of them look at the whole system, with boundaries similar to Figure 3.6. This includes all the physical elements, such as the inverter, the cables and the metal frame that encloses the solar cells, as well as the installation, transport, etc. However, the Solar solution only requires a solar cell and the associated boundaries needed for this LCA is included in the area outlined by the red dashes.

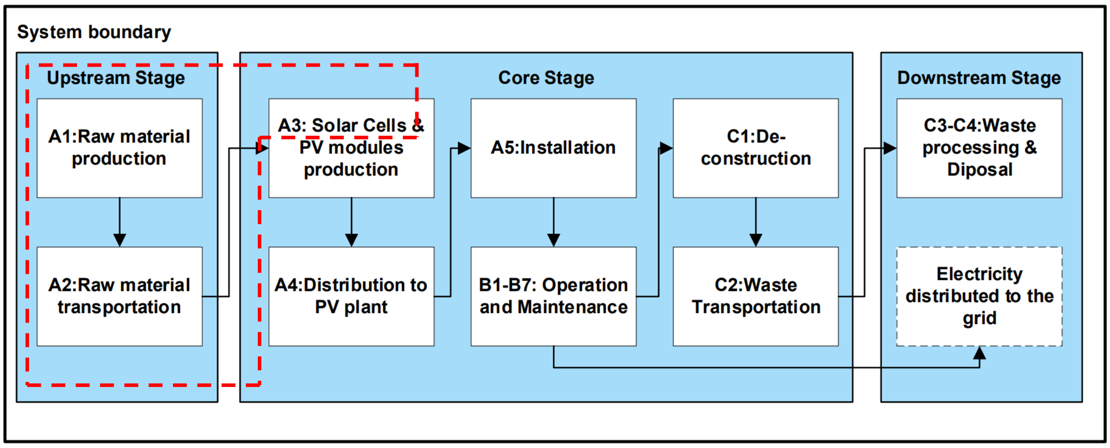

Figure 3.6: Typical system boundaries for an LCA of solar module. The area delimited by the red dashes is the relevant part of the boundaries for this study, adapted from [68].

The conclusion of these studies is often that, depending on the category of impact, most of the flows in the system boundaries have relevant impact [68][69].

In order to avoid overestimating the impacts of the solar cell, it is necessary to find a study that either displays the results by production stage, to extract the values linked to the solar cell alone, or that studies the impact of the cells separately from the rest.

A state of the art was done on the LCA of solar cells. It is summarized in Table 3.6.

Table 3.6: State of the art of environmental impact of Solar panels: a comparative, non-exhaustive table.

Source	Technology	Functional unit	Reference flow	LCIA method	System boundaries	GWP kgCO_2-eq./kWh	Additional results	Data for cell
Hong et al., 2016 [70]	multi-Si PV cell	1 kWp multi-Si PV cell production	N/A	IMPACT2002+ method	Cradle-to-gate	0.0561	1840 kgCO_2eq/kWp	No
Wu et al., 2017[71]	multi-Si PV module	N/A	N/A	N/A	Cradle-to-gate	0.0367	N/A	No
Stamford et al., 2018 [72]	mono-Si and multi-Si PV panel	1 kWh of electricity generated at the installation	PV system of 3 kWp	CML	cradle-to-grave	Mono-Si: 0.0285-0.0346 Multi-Si: 0.0249-0.0287	N/A	No
Galley et al., 2019 [60]	DISC	1 kWh of electricity production	PV system of 3 kWp	ReCiPE and EF3.0	Crade-to-grave	0.0291	3.09 kgCO_2-eq./cell	Yes
Trina Solar Science & Technology, 2020 [68]	mono-Si PV module	1 kWh of electricity generated	TSM-DE15M(II), TSM-DE17M(II)	EN 15804+A2:2019 (version 1.00) &TRACI	Cradle-to-grave	0.0172	N/A	No
Müller et al., 2021 [73]	mono-Si PV	1 kWp of nominal module power and 1 kWh of produced electricity	5.052 and 5.156 m^2/kWp	IPCC 2013 and EF 3.0	Cradle-to-grave excluding use phase and balance of system	0.0129 to 0.0299	420 to 810 kgCO_2eq/kWp	Yes
Fthenakis et al., 2021 [74]	mono-Si and multi-Si PV systems	13,615 and 14,797 MJ/kWp	N/A	CML	N/A	0.017 to 0.043	1010 to 1087 kgCO_2eq/kWp	No
Lundmark et al., 2022 [69]	mono-Si PV module	1 kWh net of electricity generated	RSM110-8-560M and RSM120-8-610M	N/A	Cradle-to-grave, except use by end consumers	0.015 to 0.016	N/A	No
Alam et al., 2023 [75]	mounted PV system using mono-Si panels	1 kWh of electricity production	N/A	TRACI 2.1	Cradle-to-gate	0.0791	N/A	No

The Table 3.6 does not display all the papers that have been accessed and reviewed, as most were deemed irrelevant due to insufficient information, the results not being shared in a manner suitable for this research, or the lack of a proper methodology.

Two papers are particularly noteworthy, from Müller et al. [73] and Galley et al. [60].

The first one stands out by the technology it studies, similar to that of the sensor manufactured by Dryad and representative of the majority of PV cells worldwide [67][76], and by the functional unit and reference flow used. In fact, they are such that it is possible to relate the values to the system evaluated in this thesis without having to resort to too many assumptions and therefore reduce the error on the impact of the solar cell. Unfortunately, the paper does not provide its results in any form other than figures, apart from the climate change, making it impossible to use them here.

The latter stands out for its application of the LCA methodology and its transparency in communicating the results it obtains. All the stages in the life cycle are described in detail, along with their respective results, and the solar cell's results are highlighted, making them easier to use in the scenario presented in this thesis. The issue, and not the least, is that this paper studies an innovative technology, the double side contacted cells with innovative carrier-selective contacts (DISC). The wafer used in the DISC is made of the same material as a monocrystalline silicon solar cell, i.e., silicon [77]. Furthermore, Galley et al. compare the LCIA results of the DISC production to the impacts of other mono-Si technologies, Heterojunction Technology (HJT) and Passivated Emitter and Rear Contact (PERC) solar cells in Figure 3.8. The results from the two other technology are not sourced. Four scenarios are observed and the comparison of their results is presented is Figure 3.9.

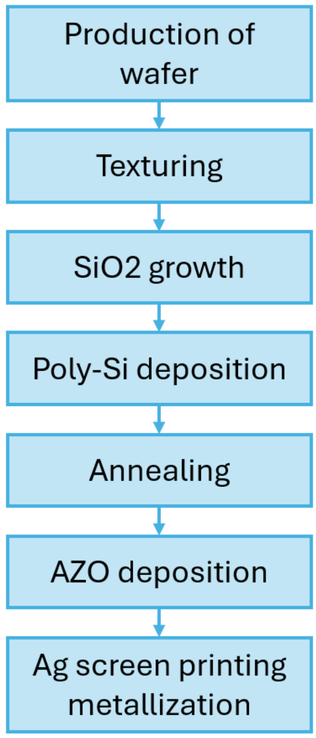

Figure 3.7: Process steps for the production of one cell in [60] for the DISC 1.1 scenario, inspired by the aforementioned document.

The Figure 3.8 shows that the results of the DISC 1.2 scenario are closer to the results of the two mono-Si. In addition, the Figure 3.9 shows that the DISC 1.1 results are slightly smaller than those of DISC 1.2. Combining the two information, DISC 1.1 seems to be the best scenario to choose.

In Table 3.7, it appears that the wafer production is the predominant part of solar cell production. It accounts for 82 to 98.5% of the total, depending on the category, except for two. The terrestrial eutrophication is influenced by the wafer at 58%, the *Poly-Si deposition* at 17.3% and the *Ag screen metallisation* at 21.2%, and the metal scarcity is influenced by the wafer à 38% and the *Ag screen metallisation* at 57.44% [60].

In addition, two observations can be made. As all solar cells technologies undergo the wafer production in their manufacturing process and that the HJT and PERC, from Figure 3.8 are close in results from the DISC 1.1, it indicates that the reference can be used and will at worst represent an upper bound to the impacts of the solar cell. Moreover, the GWP/kWh of this scenario is in the range of the results from other LCA models, as seen in Table 3.6.

In light of these analyses, the scenario DISC 1.1 from Galley et al. [60] has been selected as the reference for the production flow of solar cells. The downside of this scientific paper is the absence of uncertainty analysis and the assumption for the manufacturing location, i.e., Europe, as China is the main producer of mono-Si solar cells as of today [67]. The latter will be subject to a scenario analysis.

The energy storage is made of two SCs of 3.2g and capacitance of 10 F each.

Since LCA models for SCs are not broadly available at the time of writing, and it is necessary to find an LCA using the same LCIA methods to have a correct assessment, the research paper from Cossutta et al. [58] is chosen for the reference.

Cossutta et al. perform an LCA with a functional unit of a rack of 5 SCs with capacitance of 5F. It would have been better to scale the flow on the mass of the SCs, but such information was not given by Cossutta et al. [58], therefore the only possible way to scale the SC was on its capacitance.

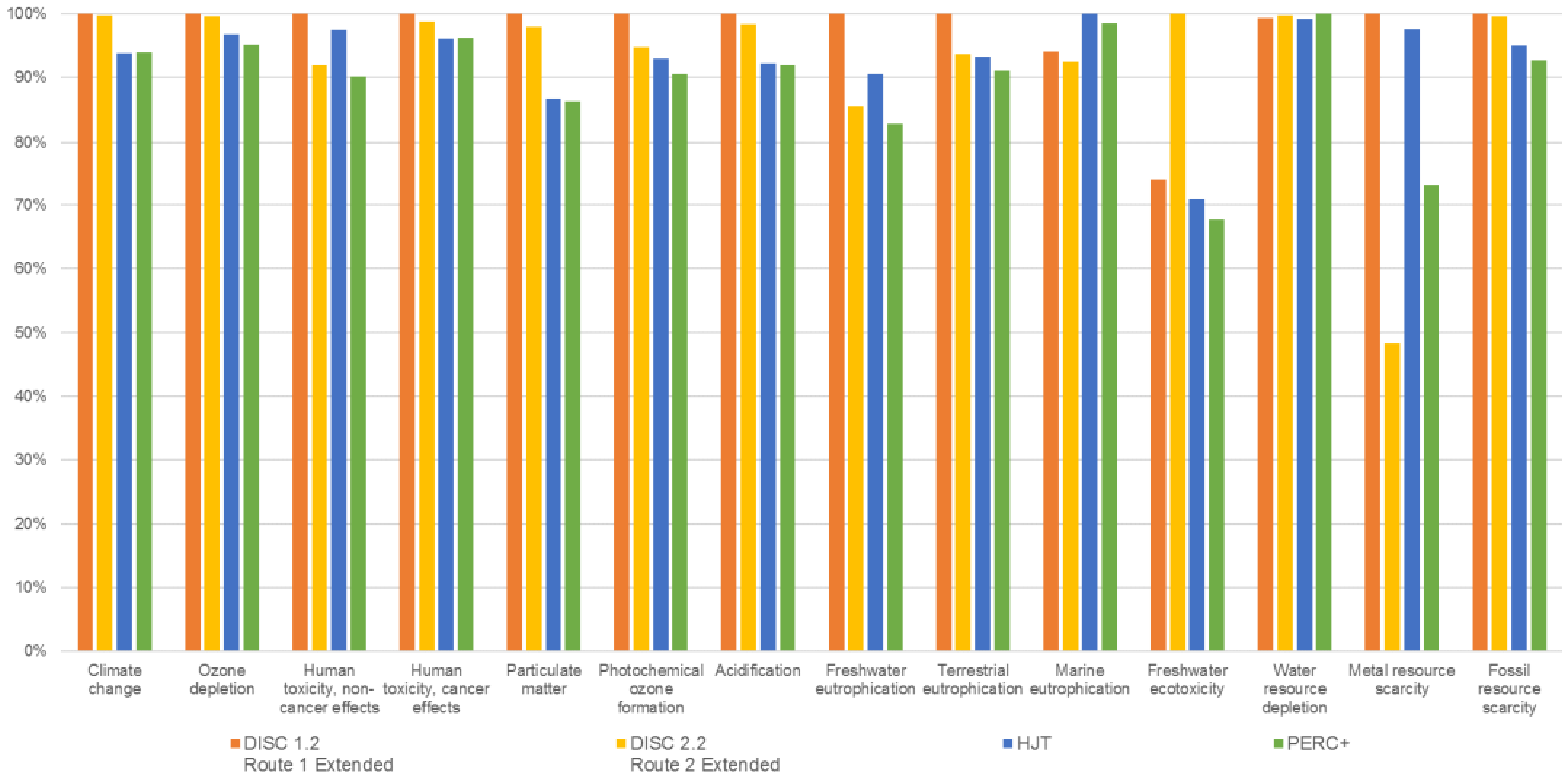

Figure 3.8: From [60], shows the differences in the multi-impact category cradle-to-gate LCIA results between two DISC scenarios, HJT. *Galley et al. do not share the reference from which they use the results for HJT and PERC+.*

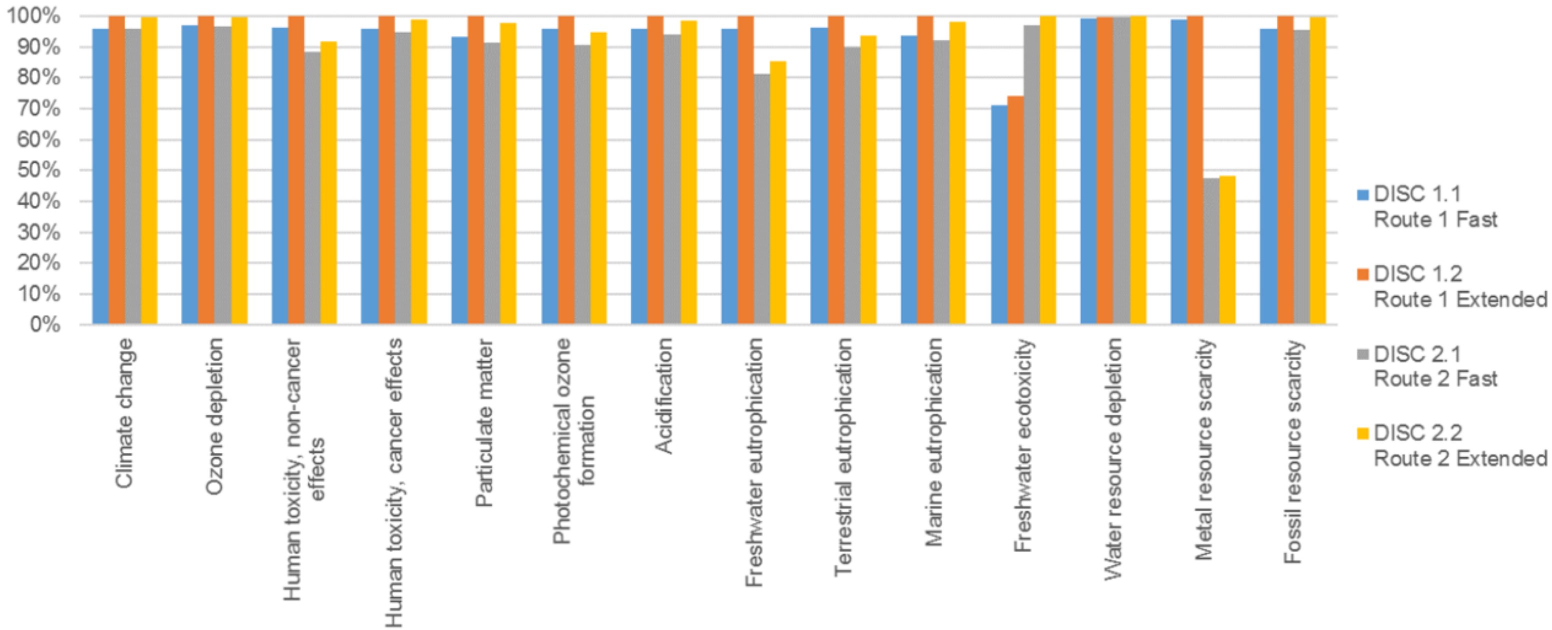

Figure 3.9: Comparison of the multi-impact category cradle-to-gate LCIA results of the four scenarios from [60].

Table 3.7: Comparison between the LCIA results of the wafer production and the total production of the cell for the DISC 1.1 scenario, adapted from Galley et al. [60].

Impact categories	**Units**	**Production of wafer**	**Total for the cell**	**Percentage of the total due to the wafer production [%]**
Climate change	[kg CO_2 eq.]	2.75	3.09	89.0
Ozone depletion	[kg CFC-11 eq.]	2.99×10^{-7}	3.31×10^{-7}	90.3
Human toxicity non-cancer	[CTUh]	2.32×10^{-7}	3.01×10^{-7}	77.1
Human toxicity cancer	[CTUh]	3.32×10^{-8}	3.70×10^{-8}	89.7
Photochemical ozone formation	[kg NMVOC eq.]	5.8×10^{-3}	6.98×10^{-3}	83.1
Acidification	[molc H+ eq.]	1.41×10^{-2}	1.65×10^{-2}	87.0
Terrestrial eutrophication	[molc N eq.]	2.55×10^{-4}	4.36×10^{-4}	58
Freshwater eutrophication	[kg P eq.]	2.34×10^{-2}	2.83×10^{-2}	82.7
Marine eutrophication	[kg N eq.]	2.54×10^{-3}	2.95×10^{-7}	86.1
Freshwater ecotoxicity	[CTUe]	8.86×10^{-1}	1.09	81.3
Water resource depletion	[m3 water eq.]	8.92×10^{-2}	9.06×10^{-2}	98.5
Metal resource scarcity	[kg Cu eq.]	6.44×10^{-3}	1.68×10^{-2}	38
Fossil resource scarcity	[kg oil eq.]	7.28×10^{-1}	8.2×10^{-1}	88.8

Battery

A similar issue to that of the solar cell and SC came for the battery modelling in GaBi. Indeed, no process existed to represent the flow of a battery.

But before deciding on how to represent this flow, it is necessary to dimension the battery required to meet the needs of the Battery solution. The main variable in that calculation is the power consumed by the sensor. Unfortunately, the values given in the specifications of Dryad do not apply here, as the solar panel used in the Solar solution is oversized to generate enough power in the shaded conditions of a forest, as mentioned in [53]. The average power consumption of the sensor will be calculated using the datasheet provided in the BoM of Dryad. Due to the NDA, the detailed datasheets will not be shared here but the important parameters, such as power consumption, will.

After a detailed review of the datasheets, it appears that the gas sensor and the MCU dominate the power consumption of the sensor.

The **gas sensor** passes through several modes during operation, each with its own average current consumption. Fortunately, Bosch discloses the electric charge for a standard scan of the sensor of 0.18 mAh, at 3.6 V, and a scan takes 10.8s. The sleep mode has an average current consumption of 3.7 µA. The gas sensor in Dryad application senses its surroundings every minute, meaning it is in active mode 18% of the time. The assumption is made that the gas sensor power consumption in sleep mode is insignificant in regard to the overall power consumption. The average power consumption of the gas sensor is assumed to be 0.648 [mWh] [54].

The **MCU** has two operating modes, active and standby. During its active mode, it consumes 15 mA at 10 dBm or 87 mA at 20 dBm. In the absence of information on the length of the packets sent by the Dryad software, a communication time of 10 s was assumed. However, the communication frequency of the Wildfire sensor is every two hours. The same metric is used for fair comparison. The standby mode consumes 360 nA and is the main mode of the MCU as it respresents 99.86% of the time it spends.

Using the values from the previous lines, the equation to determine the average power consumption of the sensor is:

$$P_{tot} = P_{gas} + P_{MCU}$$

With:

$$P_{gas} = 0.648[mW]$$

and

$$P_{MCU} = (87 \times 0.0014 + 360\text{x}10^{-6} \times 0.9986) * 3.6[V] = 0.435[mW].$$

Combine it all to obtain:

$$P_{tot} = 1.083[mW] \tag{3.1}$$

The battery must last ten years. Taking into account the average consumption of the sensor, a battery with a capacity of **26.38 Ah**, at 3.6V, is required to fullfil the needs of the sensor, which consumes 93.6 [J/day].

The criteria of selection for the battery are: a high density of energy, a low self-discharge rate and a high capacity. The choice of battery compound will be directed towards Lithium batteries, as they have a much greater power density [34]. The selected batteries are ones found available on the market [78].

Table 3.8: Non-rechargeable lithium/thionyl chloride battery (LTC) technical data from [78].

Parameter	**Value**
Nominal capacity @ 4 mA, to 2 V [Ah]	19
Nominal voltage [V]	3.6
Weight [g]	93
Power density [Wh/kg]	408.6
Maximum recommended continuous current [mA]	100
Dimensions [cm^3]	⌀3,2 x 6,1
Self-discharge rate [%/year]	0.7

This battery answers to the requirements of the sensor. With the information of Table 3.8, it appears that only one battery will not be sufficient to supply the sensor for 10 years, two will be needed. Taking this and the discharge rate into account, the required capacity is 14% higher — 0.07% for 10 years x2 — than the calculated one: **30.07 Ah**.

Similarly to the SCs, LCA models for special types of Lithium-Ion batteries, are not broadly available at the time of writing and fewer still study several impact categories while sharing their results in a way that makes them usable, i.e., in tables or with precise results in figures. The initial route taken was to take the results of several scientific papers and average them out. Unfortunately, that was not possible due to lack of sufficient sources. Therefore only one study was taken as reference, from Eracka et al. [59], which attempts to close the gaps in LCA of lithium-ion batteries.

The battery studied is a rechargeable Lithiuim-titanate-oxide (LTO) battery. The functional unit is 1 Wh of cell energy capacity and the referenc flow is one single cell weighing 0.54 kg, with a rated capacity of 20 Ah at 3.7 V, and with an energy density of 141 Wh/kg.

The results are recalculated proportionally to the weight energy density difference then scaled to the weight of the battery from Table 3.8.

UAV

All results for UAV solution on have been calculated on the basis that the batteries are recharged every two months. This is probably the upper limit, but a sweet spot for recharging frequency has yet to be found. On the one hand, the amount of diesel burned by the car transporting the UAV is high, but on the other, the battery is small. The question is which dominates more. A sensitivity analysis will be performed by varying this frequency.

Table 3.9: Key parameters of the UAV solution.

Parameter	**Value**
Flight range [km]	2
Vertical speed [m/s]	10 [1]
Horizontal speed [m/s]	19.5[1]
Mass [g]	170[1]
Flying life [h]	400[1]
Flying height [m]	20
Landing height [m]	3
Averaged maximal horizontal distance [m]	1125 [2]

[1] From [56].
[2] $\frac{0.7*1000+0.1*2000}{0.8}$, based on the functional unit.

Two parts of production of the UAV solution flow needs to be discussed here: the battery dimensions and the share of UAV allocated to the reference flow.

The battery selected is a lithium-titanate or lithium-titanium-oxide (LTO) battery [79]. This choice was based on the conclusions of Van Mulders et al. [56] that the combination of fast charge time, low self-discharge and relatively high energy density was appropriate for this particular application.

Table 3.10: Rechargeable lithium-titanate-oxide battery (LTO) technical data from [79].

Parameter	**Value**
Nominal capacity [mAh]	500
Nominal voltage [V]	2.4
Chargin Rate	20C
Cycle life for 1C and above	> 5000 times
Weight [g]	16.6
Power density [Wh/kg]	72.3
Dimensions [cm^3]	⌀1.4 x 5
Self-discharge rate [%/year]	3

The flow of this battery was, similarly to the Battery solution, not implemented in the database provided in GaBi. The study described for the previous solution is also used for the UAV solution, and the results are scaled to the weight of the battery selected. Using the result from Equation 3.1 and the self-discharge rate of 3%/year, which results in 0.5% for 2 months, for the rechargeable battery from [79], the capacity needed for the battery is: 0.442 [Ah] as the battery nominal voltage is 2.4 V. The lower voltage compared to the Battery solution is not an issue, as components from the sensor can function on a range of voltage, from 1.8 to 3.6V.

A battery of 500mAh weighs 16.6g, as stated in the technical data from [79], and will be taken as reference.

The battery reference will be the same for the Battery and UAV solutions, even though they have different requirements. The results are recalculated proportionally to the weight energy density difference then scaled to the weight of the battery from Table 3.10.

The share of UAVs depends on the lifetime of the UAV, which is 400 hours, and the time it takes to fly to, find and land on the sensor.

The time per flight, t_{flight}, is calculated as follows:

$$t_{flight} = (t_{vert,1} + t_{hor} + t_{vert,2}) \times 2 + 60[s]$$

with:

$$t_{vert,1} = \frac{h_1}{V_{vert}},\ t_{hor} = \frac{d_{hor}}{V_{hor}} \text{ and } t_{vert,2} = \frac{h_1 - h_2}{V_{vert}}.$$

The 60s added to t_{flight} refers to the time it takes for the UAV to find the sensor, as it will not land directly on the sensor. In fact, Dryad explains that when a sensor is deployed, a location is given on their map with a 20m radius around that point, as there may not be a tree at the specific location [53], and the UAV pilot or AI autopilot will need some time to find the sensor within that radius.

Using the values from Table 3.9, t_{flight} is found to be 181.1 s.

With a recharging frequency of 2 months, the UAV will perform 60 flights per sensor, giving a total of t_{flight} of 181 min 6s dedicated to one sensor in ten years. During its lifetime, a UAV will service 132.5 sensors. Therefore, the share of UAVs allocated to a sensor is $\mathbf{7.55}\times10^{-3}$ of UAV production.

3.2.3 Distribution

The use case is situated in the "Parc naturel régional de la Sainte-Baume", France. The entry point to the Parc is set to the small town of Auriol, located to the west of the Parc. The sensor begins its journey after being packed on the Dryad assembly line in Eberswalde, north-east Germany. The distance by car between assembly and Auriol is 1650 km, according to Google Maps.

The mean of transport to be used by the sensor must still be selected. GaBi offers different flows for truck transport, with three parameters, the energy used: CNG, diesel, petrol or electricity; the maximum payload of the truck, ranging from 1.5t to 27t; and the European emission standards it complies with, from Euro 1 to 6.

For the first, considering that 96% of the truck market share was taken by diesel trucks in 2022 [80], using a diesel-powered truck is a good assumption.

For the second parameter, it is necessary to take a different angle of view and examine the shipment to which the sensor from the reference flow will belong. The sensors are intended to cover the entire park, i.e., 84000 ha. As the total length of roads in the Parc is unknown, Dryad's scale of 0.24 sensors/ha, from [53] is used to measure the amount of sensors needed for this task. A shipment of 20160 sensors, or 2016 boxes, must be sent to cover the 84000 ha. Each box contains 10 sensors, 10 treenails and 10 spacers, and is made of cardboard. A sensor weighs 136g [53], a treenail 11.39 g, using a density of 634.1 kg/m^3 for the oakwood [81], a spacer is of negligible weight, and the cardboard, of density of 90 g/m^3 [82], necessary for the box weighs 24.73g. In total, one box weighs 1.5 kg. Multiplied by 2016, this represents a cargo of 3.024 tonnes to cover the whole park. The weight of the UAV was not included in the UAV solution distribution. Indeed, with 1 UAV for 132.5 sensors, it only adds 1.3g to the total weight of a sensor.

And finally, for the third parameter, considering the new regulation Euro 7 imposed on every new road vehicle [83], the choice of a Euro 6 truck is a good assumption.

Given the cargo to be transported, and the engine most commonly used for trucks, a diesel-powered lorry with a maximum payload of 5t respecting the Euro 6 regulation was chosen.

3.2.4 Use Phase

On entering the use phase, the deployment of the sensor has two common steps to the three solutions, with the UAV having an extra step in this phase. The first step is to transport the sensor to the location where it will be deployed, the second is to attach it to its home tree.

The "Parc naturel régional de la Sainte-Baume" can be approximated by a circle with a radius of 16 km, according to the measuring instrument of Google Maps. Using this information, the simplified average distance a sensor has to travel to reach its home tree is 16 km.

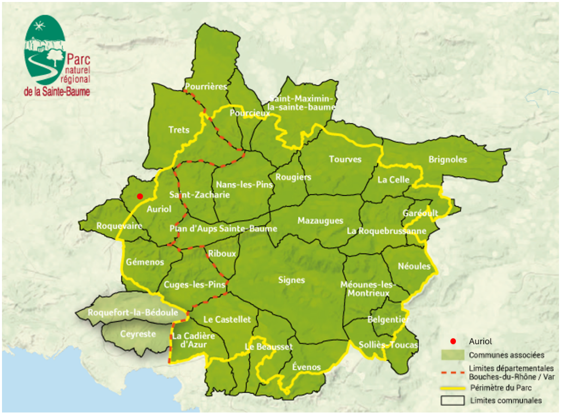

Figure 3.10: Map of the "Parc naturel de la Sainte-Baume", modified from [84]. The red dot indicates where the warehouse is located and the yellow line marks the Parc boundaries.

The dispatching is, as mentioned above, a task executed by the French forest rangers. Dryad's documentation indicates that two people (working in teams of two is recommended) can deploy between 20 and 50 devices per day [53]. The first will be considered to set the upper limit, a sensitivity analysis will be performed if the use phase appears as a hotspot in the results. The production of the car used, and the kilometres travelled from the warehouse to the tree and back, are included in the scope of the use phase. Anything else, i.e., the tools used, the commuting of the workers, the walk in the forest, etc., are excluded from the study. Thus, the parameter used to define the impacts related to the use phase is the kilometres travelled by car by the sensor. The distance (d_{sens}) allocated to a sensor is defined by the following equation:

$$d_{sens} = \frac{\text{km travelled}}{\text{number of sensors}} \tag{3.2}$$

$$\iff \boxed{d_{sens} = 1.6\ [km/sensor]}.$$

Concerning the car production, little information is disclosed on the typical car used by the "Office National des Forêts" (ONF), but a good assumption is to consider it as a city car [85]. According to Weymar et al. [86], the average mileage of such cars goes from 170 000 km to 250 000 km. An upper bound will be fixed by using 170 000 km.

The share of the car production (car_{sens}) allocated to a sensor is defined by the following equation:

$$car_{sens} = \frac{d_{sens}[km/sensor]}{\text{mileage }[km/car]} \Longleftrightarrow \boxed{car_{sens} = 9.412\text{x}10^{-6}\ [car/sensor].} \tag{3.3}$$

The round trip between the warehouse and the tree is modelled by diesel consumption, with an average consumption of 6.8 [l/100km] [87] and a density of diesel of about 0.85 [kg/l] [88].

The share of diesel consumption ($diesel_{sens}$) allocated to a sensor is defined as:

$$diesel_{sens} = consumption[l/km] \times density[kg_{diesel}/l] \times d_{sens}[km/sensor] \tag{3.4}$$

$$\Longleftrightarrow \boxed{diesel_{sens} = 0.0924\ [kg_{diesel}/sensor].}$$

These values remain unchanged for each solution.

The additional step mentioned above for the UAV solution is the recharging of the batteries. It can be divided into 3 parts: the recharging process, the UAV flight and the car driving to the location of the sensor.

The first and second parts are represented by an electricity consumption.

In [56], there are two ways to perform the WPT: while hovering or after landing on the sensor. Here, the decision has been made to land on the sensor, so the only energy needed for the UAV is for the flight. This choice is based on the battery capacity and the time taken to perform the WPT. If the battery was much smaller, the hovering would be a preferable option. All the equations and values below are taken from [56] unless otherwise stated.

$$E_{uav,overall} = 2 \times E_{uav,travel} + (\eta_{wpt})^{-1} \times E_{IoT,storage} \tag{3.5}$$

With

$$\begin{aligned} E_{uav,travel}(h_1, h_2, V_{vert}, d, V_{hor}, m) = P_{uav}(V_{vert}, m) \times \frac{h_1}{V_{vert}} + P_{uav}(V_{hor}, m) \times \frac{d}{V_{hor}} \\ + P_{uav}(-V_{vert}, m) \times \frac{h_1 - h_2}{V_{vert}} \end{aligned} \tag{3.6}$$

knowing that:

$$P_{uav}(V_{hor}, m) = (c_1 + c_2) \left[\sqrt{(mg - c_4(V_{hor}\cos\alpha)^2)^2 + (c_3 V_{hor}^2)^2} \right]^{\frac{3}{2}} + c_3 V_{hor}^3$$

$$P_{uav}(V_{vert}, m) = k_1 mg \left[\frac{V_{vert}}{2} + \sqrt{\left(\frac{V_{vert}}{2}\right)^2 + \frac{mg}{k_2^2}} \right] + c_2 (mg)^{\frac{3}{2}}.$$

Table 3.11: Constant parameters for the equations on one side, variable parameters on the other.

Parameter[1]	**Value [-]**	**Parameter**	**Value**
k_1	1.560	V_{vert} [m/s]	10
k_2	0.467	V_{hor} [m/s]	19.5
c_1	3.428	m [g]	170
c_2	9.451	h_1 [m][2]	20
c_3	-0.0037	h_2 [m] [2]	3
c_4	-0.0044	d [m][2]	1125

[1] Custom UAV parameters extracted from real-life experiments in [56].
[2] Assumptions from Table 3.9.

The angle of attack, α, is assumed to be 0, as the author of [56] was unable to extract any useful data from the UAV measurements. This assumption is used here, so $cos\alpha$ is equal to 1.

Adding all this up, $E_{uav,travel} = 3.63[kJ]$. Using the value from section 3.2.2, $E_{IoT,storage} = 3.82[kJ]$ and assumed η_{wpt} to be equal to 50% based on [56], with Equation 3.5, the overall electricity consumption used to fly the UAV and charge the batteries is:

$$\boxed{E_{uav,overall} = 14.9[kJ/trip].}$$

Similar to the deployment, the third part is assimilated to a diesel consumption and a car production. Equation 3.2, 3.3 and 3.4 can be reused. The number of sensors serviced per trip changes, as it takes less time to supply them than to deploy them. For this reason, d_{sens} must be revised. It depends on the time taken by a UAV to reach the sensor and do the transfer.

Firstly, the capacity of the battery is a variable because it determines the time required to perform the WPT. The capacity, in this case 3.82 kJ, is directly linked to the frequency of recharging, every two months, since this is assumed to be its upper limit, as set in the section 3.2.2.

Secondly, the flight time of the UAV is constant and is calculated in section 3.2.2 to be equal to 181.5 s, with the average maximal distance.

From [56],

$$t_{ch} = \frac{3600}{C_{rate}} \times (SoC_{target} - SoC_{initial})$$

with

$$\text{the charging rate, } C_{rate} = \frac{P_{ch,max}}{E_{node}} * 3600 = 9.42,$$

as $E_{node} = 3.82[kJ]$, from section 3.2.2, and $P_{ch,max} = 10[W]$, from[56]. SoC is the state of charging. SoC_{target} is 1 and $SoC_{initial}$ is 0.12 as the node is expected to have used 88% of the battery after each cycle and must be charged to 100%. In conclusion, t_{ch} is 336.3 [s].

The total time taken to charge a sensor is of 517.8s, 8 min 37.8s. In a 8h work day, 55.6 sensors can be supplied. Therefore, d_{sens} equals 0.57 $[km/sensor]$, car_{sens}, 3.35×10^{-6} $[car/sensor]$ and $diesel_{sens}$, 0.0329 $[kg_{diesel}/sensor]$ per cycle.

3.3 Life-Cycle Impact Assessment

The third phase to an LCA study, the Life-Cycle Impact Assessment (LCIA) translates the LCI model and all its flows into environmental scores. It stands as a section where all the results are recorded in the most understandable way to facilitate the next steps of the LCA, the sensitivity analysis and the interpretation.

This section will report the LCIA results based on the previous chapters.

Before delving into the details, some precision is needed. The paper by Galley et al. [60] examines the impacts of the solar cell. The authors chose to use the ILCD for all categories except metal and fossil depletion, using the ReCiPe method, because they had concerns about the ILCD method for characterising resource depletion impacts. This is not a concern when studying the Solar solution alone, but seemed to be an issue for the comparison. In fact, the battery impact study [59] also uses ReCiPe for metal depletion but ILCD for fossil depletion. The UAV and Battery solutions can still be compared for the metal depletion, as the battery impact study [59] uses ILCD for metal depletion but has no interest in the fossil depletion category.

Solutions will not be compared in impact categories where they do not have a similar calculation methodology, but every possible result will be displayed.

Here is a reminder of the environmental impact categories with their abbreviations, the **P** stands for "potential":

- Acidification - **AP**
- Climate Change - **GWP**
- Ecotoxicity, freshwater - **FETP**
- Eutrophication, freshwater - **FEP**
- Eutrophication, maritime - **MEP**
- Eutrophication, terrestrial - **TEP**
- Human toxicity, cancer - **HTPc**
- Human toxicity, non-cancer - **HTPnc**
- Ozone depletion - **ODP**
- Photochemical ozone formation, human health - **HOFP**
- Resource use, mineral and metals - **SOP**
- Water use - **WCP**

3.3.1 Cradle-to-grave LCIA Results

LCI section

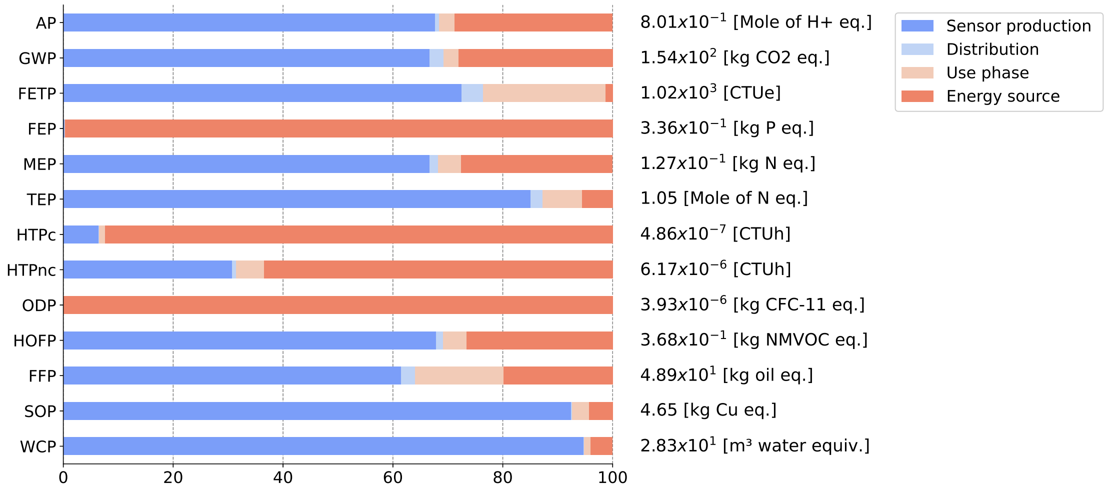

Figure 3.11: Multi-impact category LCIA cradle-to-grave results, excluding EoL - For the Solar solution in % by section of the LCI, per km of road covered.

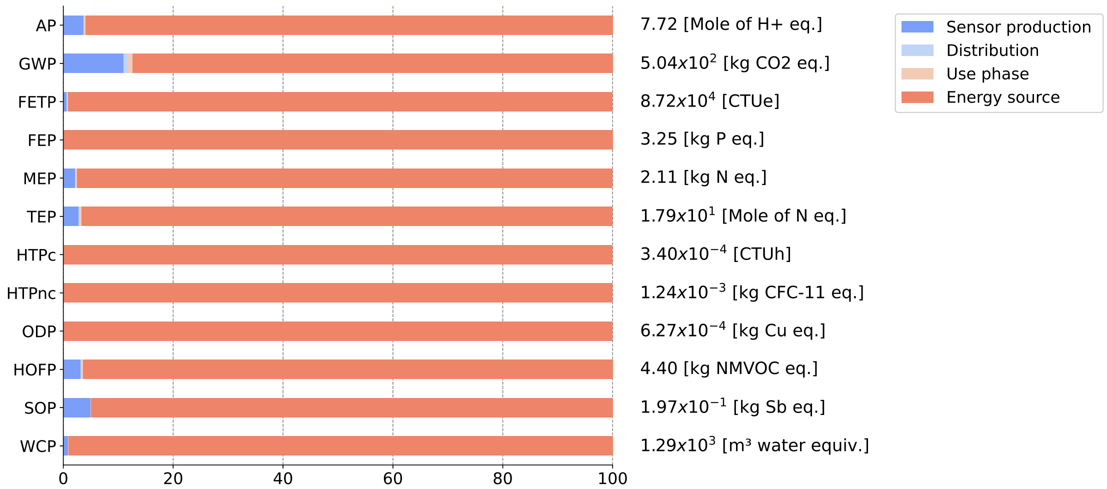

Figure 3.12: Multi-impact category LCIA cradle-to-grave results, excluding EoL - For the Battery solution in % by section of the LCI, per km of road covered.

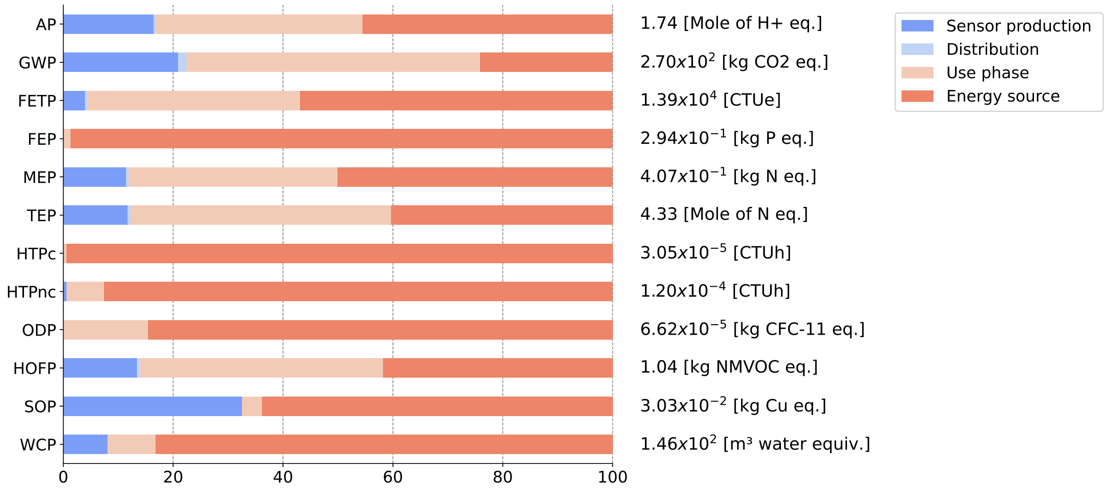

Figure 3.13: Multi-impact category LCIA cradle-to-grave results, excluding EoL - For the UAV solution in % by section of the LCI, per km of road covered.

Flow by flow

In the following figures, each component is associated with a fixed colour. The energy storage bar is light pink for all three solutions. For the UAV and Solar solutions, the energy source bar is dark grey. Only the UAV solution has a light grey bar associated with the maintenance UAV. The passive elements refer to resistors and capacitors.

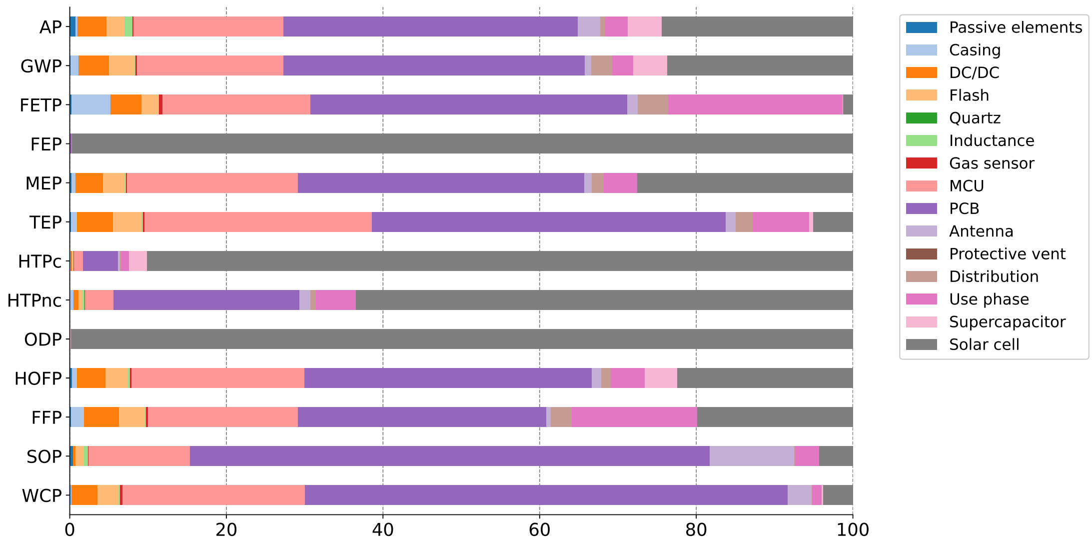

Figure 3.14: Multi-impact category LCIA cradle-to-grave results, excluding EoL - For the Solar solution in % by process, per km of road covered.

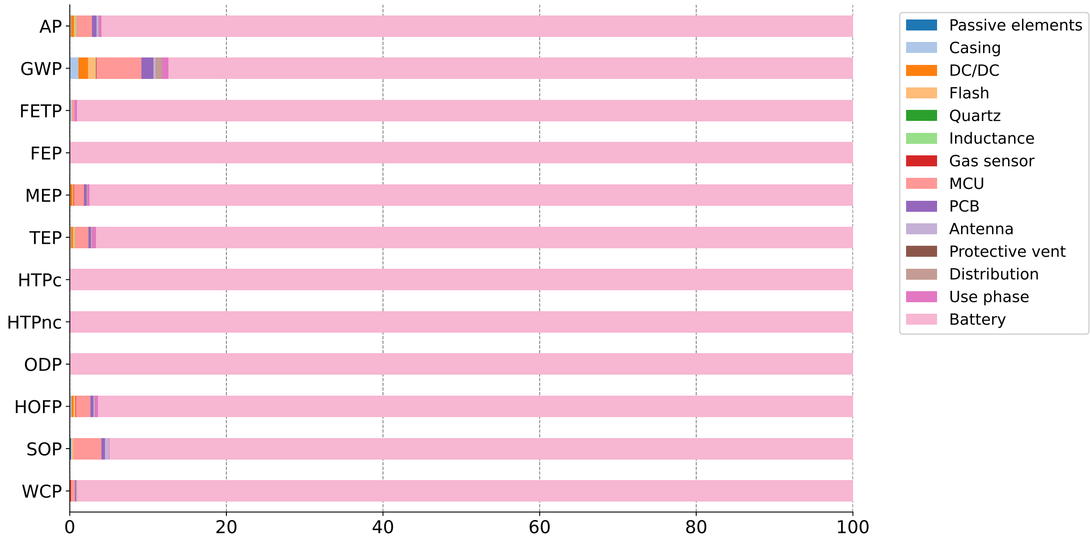

Figure 3.15: Multi-impact category LCIA cradle-to-grave results, excluding EoL - For the Battery solution in % by process, per km of road covered.

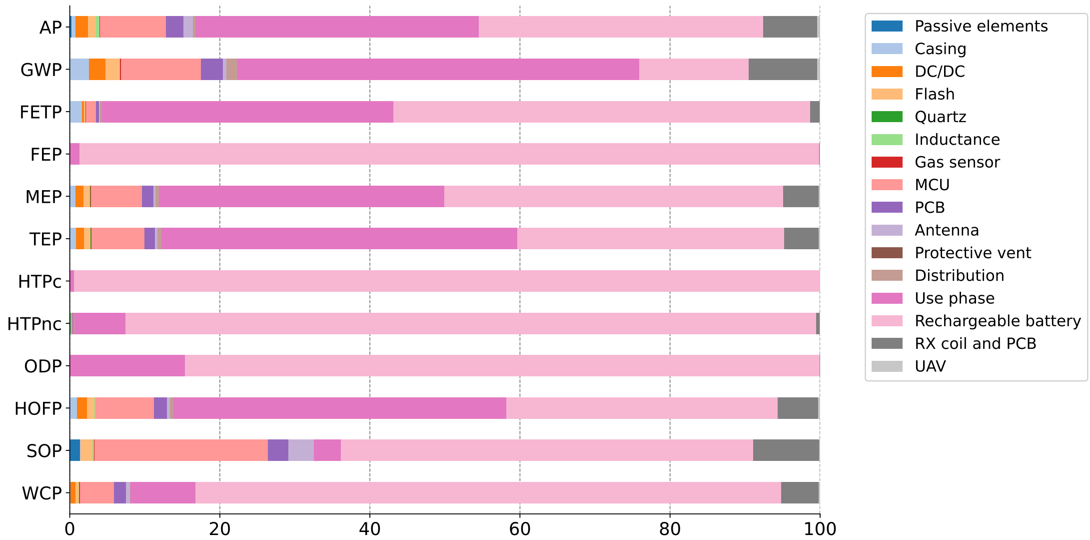

Figure 3.16: Multi-impact category LCIA cradle-to-grave results, excluding EoL - For the UAV solution in % by process, per km of road covered.

3.3.2 Comparison Between the Solutions

Figure 3.17: Multi-impact category LCIA cradle-to-grave results, excluding EoL - Comparison between the three solutions, per sensor. Results are normalised to the Battery solution

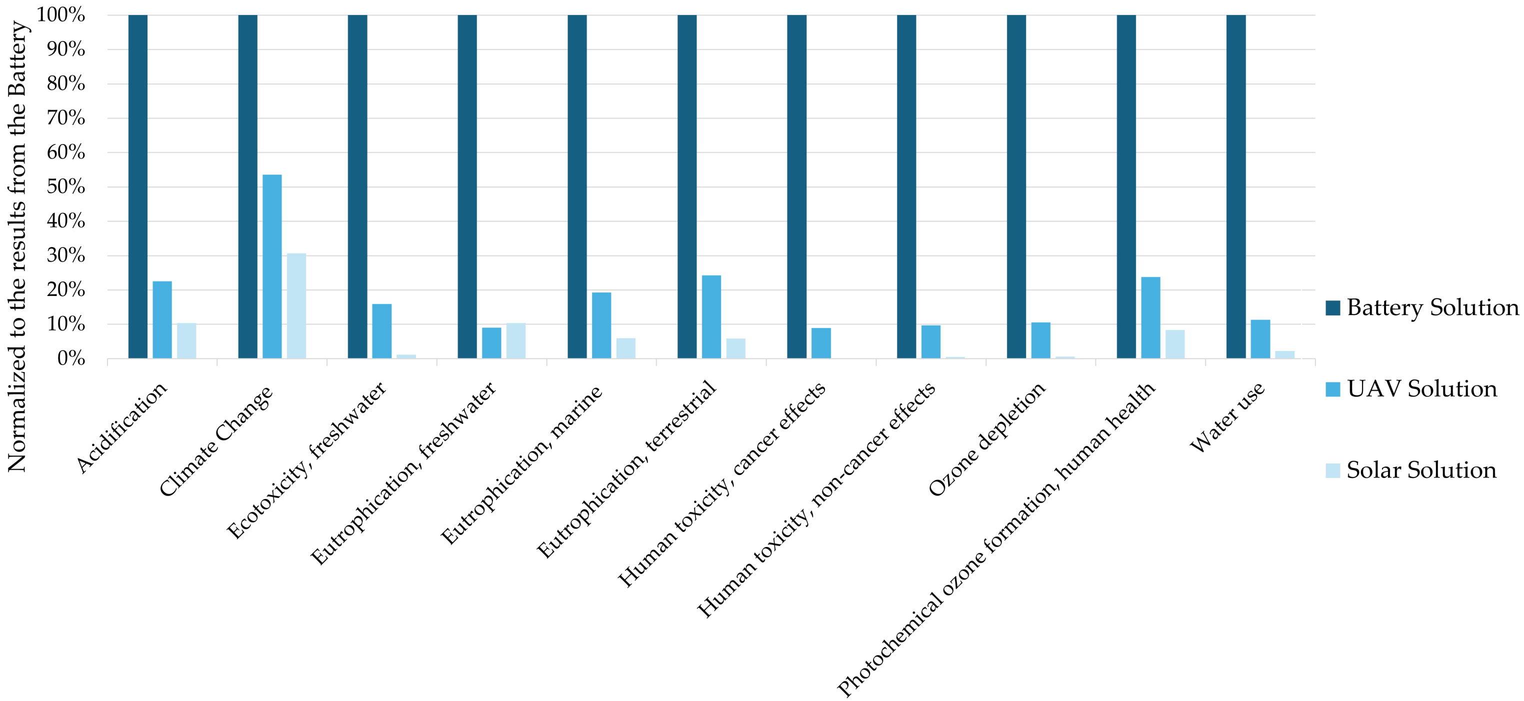

Figure 3.18: Multi-impact category LCIA cradle-to-grave results, excluding EoL - Comparison between the UAV and Solar solutions, per sensor. Results are normalised to the UAV solution, apart for the freshwater eutrophication to which they are normalised to the Solar solution

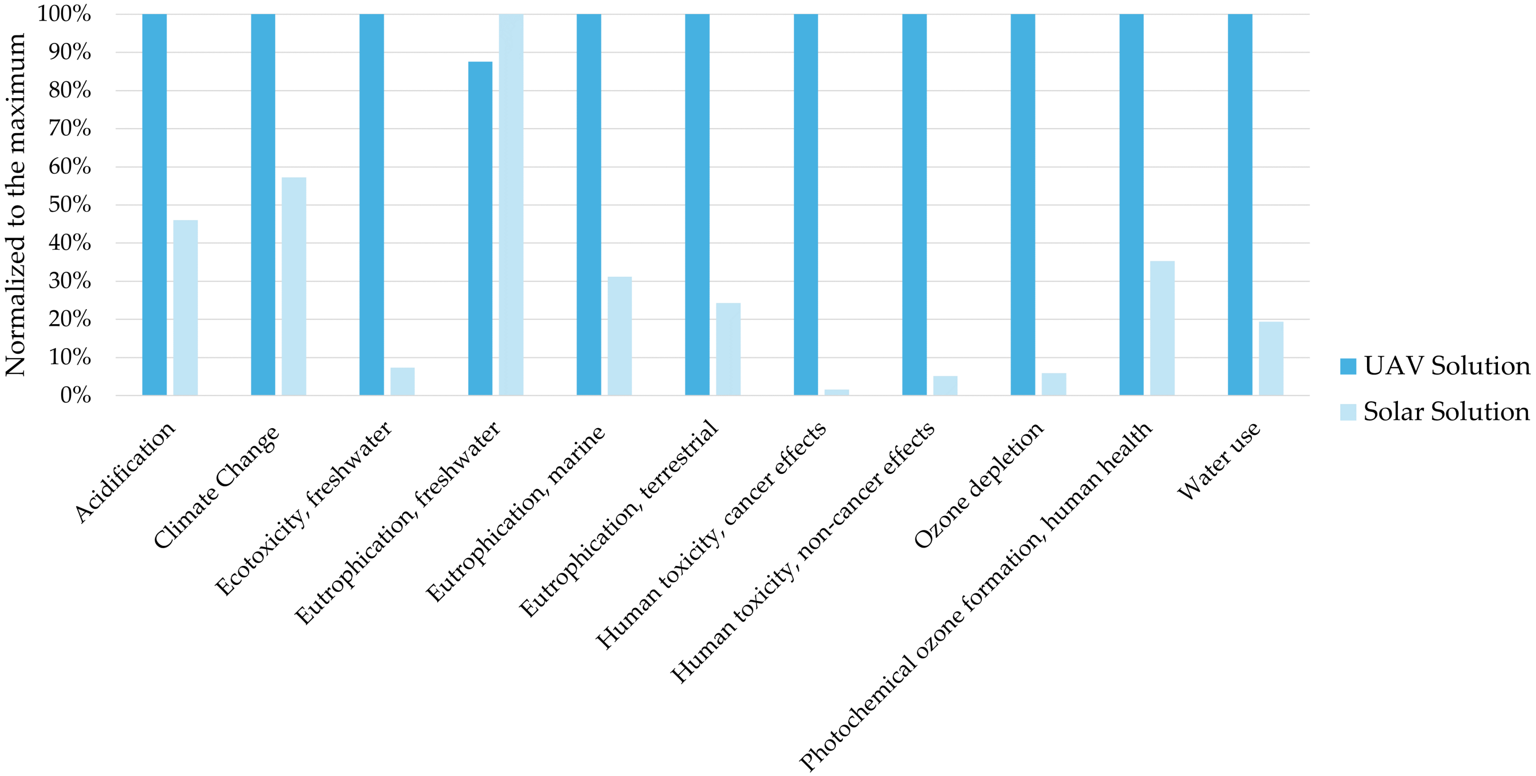

Table 3.12: LCIA results cradle-to-grave - comparison of the three scenarios per km of road covered.

	Units	**Solar solution**	**Battery Solution**	**UAV Solution**
Acidification	[Mole of H+ eq.]	0.80	7.72	1.74
Climate Change	[kg CO_2 eq.]	154.0	504.0	270.0
Ecotoxicity, freshwater	[CTUe]	1.02×10^{3}	8.72×10^{4}	1.39×10^{4}
Eutrophication, freshwater	[kg P eq.]	0.34	3.25	0.29
Eutrophication, marine	[kg N eq.]	0.13	2.11	0.41
Eutrophication, terrestrial	[mole N eq.]	1.05	17.87	4.33
Human toxicity, cancer	[CTUh]	4.86×10^{-7}	3.40×10^{-4}	3.05×10^{-5}
Human toxicity, non-cancer	[CTUh]	6.17×10^{-6}	1.24×10^{-3}	1.20×10^{-4}
Ozone depletion	[kg CFC-11 eq.]	3.93×10^{-6}	6.27×10^{-4}	6.62×10^{-5}
Photochemical formation, human health	[kg NMVOC eq.]	0.37	4.40	1.04
Water use	[m^3 water equiv.]	28.32	1.29×10^{3}	146.0

Table 3.13: Detailed results for the Solar solution, per sensor.

	Units	Sensor production	Distribution	Use phase	Energy source	Total
Acidification	[Mole of H+ eq.]	0.54	5.24×10^{-3}	2.29×10^{-2}	0.23	0.80
Climate Change	[kg CO2 eq.]	1.03×10^{2}	4.07	4.12	43.4	1.54×10^{2}
Ecotoxicity, freshwater	[CTUe]	7.41×10^{2}	39.6	2.28×10^{2}	13.2	1.02×10^{3}
Eutrophication, freshwater	[kg P eq.]	8.45×10^{-4}	9.50×10^{-6}	1.64×10^{-4}	0.34	0.34
Eutrophication, marine	[kg N eq.]	8.45×10^{-2}	1.93×10^{-3}	5.38×10^{-3}	3.49×10^{-2}	0.13
Eutrophication, terrestrial	[Mole of N eq.]	0.89	2.30×10^{-2}	7.55×10^{-2}	5.88×10^{-2}	1.05
Human toxicity, cancer effects	[CTUh]	3.11×10^{-8}	7.98×10^{-10}	4.99×10^{-9}	4.49×10^{-7}	4.86×10^{-7}
Human toxicity, non-cancer effects	[CTUh]	1.90×10^{-6}	4.05×10^{-8}	3.14×10^{-7}	3.92×10^{-6}	6.17×10^{-6}
Ozone depletion	[kg CFC-11 eq.]	5.59×10^{-10}	9.94×10^{-13}	2.73×10^{-12}	3.93×10^{-6}	3.93×10^{-6}
Photochemical ozone formation, human health	[kg NMVOC eq.]	0.25	4.61×10^{-3}	1.58×10^{-2}	9.79×10^{-2}	0.37
Fossil depletion	[kg oil eq.]	30.0	1.29	7.85	9.71	48.9
Metal depletion	[kg Cu eq.]	4.30	5.24×10^{-3}	0.14	0.20	4.65
Water use	[m^3 water equiv.]	26.8	2.12×10^{-2}	0.34	1.13	28.32

Table 3.14: Detailed results for the Battery solution, per km of road covered.

	Units	Sensor production	Distribution	Use phase	Energy source	Total
Acidification	[Mole of H+ eq.]	0.28	5.24×10^{-3}	2.30×10^{-2}	7.41	7.72
Climate Change	[kg CO2 eq.]	55.2	4.07	4.12	4.41×10^{2}	5.04×10^{2}
Ecotoxicity, freshwater	[CTUe]	5.18×10^{2}	39.60	2.28×10^{2}	8.64×10^{4}	8.72×10^{4}
Eutrophication, freshwater	[kg P eq.]	1.80×10^{-4}	9.50×10^{-6}	1.64×10^{-4}	3.25	3.25
Eutrophication, marine	[kg N eq.]	4.60×10^{-2}	1.93×10^{-3}	5.38×10^{-3}	2.06	2.11
Eutrophication, terrestrial	[Mole of N eq.]	0.50	2.30×10^{-2}	7.55×10^{-2}	17.27	17.87
Human toxicity, cancer effects	[CTUh]	1.35×10^{-8}	7.98×10^{-10}	4.99×10^{-9}	3.40×10^{-4}	3.40×10^{-4}
Human toxicity, non-cancer effects	[CTUh]	6.98×10^{-7}	4.05×10^{-8}	3.14×10^{-7}	1.24×10^{-3}	1.24×10^{-3}
Ozone depletion	[kg CFC-11 eq.]	3.30×10^{-10}	9.94×10^{-13}	2.73×10^{-12}	6.27×10^{-4}	6.27×10^{-4}
Photochemical ozone formation, human health	[kg NMVOC eq.]	0.14	4.61×10^{-3}	1.58×10^{-2}	4.24	4.40
Resource use, mineral and metals	[kg Sb eq.]	9.88×10^{-3}	2.92×10^{-7}	4.91×10^{-5}	0.19	0.20
Water use	[m^3 water equiv.]	11.74	2.12×10^{-2}	3.41	1.27×10^{3}	1.29×10^{3}

Table 3.15: Detailed results for the UAV solution, per km of road covered.

	Units	Sensor production	Distribution	Use phase	Energy source	Total
Acidification	[Mole of H+ eq.]	0.29	5.24×10^{-3}	0.66	0.79	1.74
Climate Change	[kg CO2 eq.]	56.4	4.07	1.44×10^{2}	65.1	2.70×10^{2}
Ecotoxicity, freshwater	[CTUe]	5.58×10^{2}	39.6	5.39×10^{3}	7.89×10^{3}	1.39×10^{4}
Eutrophication, freshwater	[kg P eq.]	1.85×10^{-4}	9.50×10^{-6}	3.75×10^{-3}	0.20	0.29
Eutrophication, marine	[kg N eq.]	4.66×10^{-2}	1.93×10^{-3}	0.15	0.20	0.41
Eutrophication, terrestrial	[Mole of N eq.]	0.51	2.30×10^{-2}	2.06	1.75	4.33
Human toxicity, cancer effects	[CTUh]	1.38×10^{-8}	7.98×10^{-10}	1.56×10^{-7}	3.03×10^{-5}	3.05×10^{-5}
Human toxicity, non-cancer effects	[CTUh]	7.18×10^{-7}	4.05×10^{-8}	8.17×10^{-6}	1.11×10^{-4}	1.20×10^{-4}
Ozone depletion	[kg CFC-11 eq.]	3.42×10^{-10}	9.94×10^{-13}	1.02×10^{-5}	5.60×10^{-5}	6.62×10^{-5}
Photochemical ozone formation, human health	[kg NMVOC eq.]	0.14	4.61×10^{-3}	0.46	0.44	1.04
Resource use, mineral and metals	[kg Sb eq.]	9.88×10^{-3}	2.92×10^{-7}	1.10×10^{-3}	1.94×10^{-2}	3.03×10^{-2}
Water use	[m^3 water equiv.]	11.8	2.12×10^{-2}	12.7	1.21×10^{2}	1.46×10^{2}

UAV

Table 3.16: Environmental impact results of the UAV in the UAV solution per sensor, from [56]

Impact Categories	**Units**	**Total for the UAV**
Climate Change	[kg CO_2 eq.]	1.23×10^{-2}
Ozone Depletion	[kg CFC-11 eq.]	7.18×10^{-14}
Human Toxicity Non-cancer	[CTUh]	2.39×10^{-10}
Human Toxicity Cancer	[CTUh]	4.59×10^{-12}
Photochemical Ozone Formation	[kg NMVOC eq.]	2.9210^{-5}
Acidification	[molc H+ eq.]	7.62×10^{-5}
Terrestrial Eutrophication	[molc N eq.]	1.01×10^{-4}
Freshwater Eutrophication	[kg P eq.]	1.06×10^{-7}
Marine Eutrophication	[kg N eq.]	9.54×10^{-6}
Freshwater Ecotoxicity	[CTUe]	9.49×10^{-2}
Water Resource Depletion	[m^3 water eq.]	3.23×10^{-3}
Resource use, mineral and metals	[kg Sb eq.]	4.96×10^{-7}

Table 3.17: Results for the production of SC and rechargeable battery, per sensor. As mentioned in the previous section, the SC results come from Cossutta et al.[58] and from Eracka et al.[59] for the battery.

	Units	**Supercapacitor**	**Rechargeable battery**
Acidification	Mole of H+ eq.	4.34×10^{-4}	8.26×10^{-3}
Climate Change	kg CO2 eq.	8.5×10^{-2}	0.49
Ecotoxicity, freshwater	CTUe	3.792×10^{-3}	96.4
Eutrophication, freshwater	kg P eq.	9.84×10^{-8}	3.63×10^{-3}
Eutrophication, marine	kg N eq.	N/A	2.29×10^{-3}
Eutrophication, terrestrial	Mole of N eq.	6.70×10^{-4}	1.93×10^{-2}
Human toxicity, cancer	CTUh	1.40×10^{-10}	3.79×10^{-7}
Human toxicity, non-cancer	CTUh	N/A	1.38×10^{-6}
Ionising radiation, human health	kBq U235 eq.	1.34×10^{-2}	0.47
Ozone depletion	kg CFC-11 eq.	8.56×10^{-11}	7.00×10^{-7}
Photochemical ozone formation, human health	kg NMVOC eq.	1.91×10^{-4}	4.73×10^{-3}
Primary energy demand	MJ	1.86	N/A
Mineral, fossil and ren ressource depletion	kg Sb eq	7.06×10^{-7}	2.08×10^{-4}
Water use	m^3 water equiv.	6.76×10^{-4}	1.42

3.4 Scenario Analysis

The only certitude in an LCA is that there is uncertainty. Therefore, a scenario analysis will be performed, comparing LCIA results for different flows from the LCI model.

3.4.1 Influence of the Recharging Frequency on the UAV Solution

Changing the charging frequency has five effects. Firstly, the longer the time between charges, the bigger the battery needs to be to last that long. Second, less recharging means less fuel is burned by the car to power the sensors. Thirdly, the size of the casing changes because a bigger battery means a bigger container is needed, which increases the amount of plastic needed to make it. Fourth, power consumption, which is quite complicated because a higher frequency means more UAV flights, more losses through the WPT, but less self-discharge of the battery, which is high for rechargeable batteries, i.e., 3% in [79]. Finally, a UAV has a limited lifetime of 400 hours [56], so increasing the recharging frequency means allocating more UAVs per sensor.

Seven scenarios are monitored for this comparison. The frequency will range linearly from 1 to 6 months and will also include 1 year. These changes have a direct impact on the key parameters shown in the Table 3.18. A sweet spot is observed when recharging every 2 months in Figure 3.19 once all the calculations and simulations have been done.

Table 3.18: Parameters depending on the recharging frequency and their values for the different scenarios.

	1m	**2m**	**3m**	**4m**	**5m**	**6m**	**1y**
Self-discharge Rate [%]	0.3	0.5	0.8	1	1.25	1.5	3
Battery Capacity [Ah]	0.220	0.442	0.664	0.888	1.112	1.338	2.716
Energy [kJ]	1.903	3.816	5.738	7.670	9.611	11.562	23.465
Battery Weight[1]	8.3	16.6	22	29.7	38.5	43.2	78.8
Number of Flights	120	60	40	30	24	20	10
Distance travelled [km]	68.4	34.2	22.8	17.1	13.68	11.4	5.7
Scaling Factor for Rechargeable battery	1.1707	2.3413	3.1030	4.1890	5.4302	6.0931	11.1142
Scaling Factor for UAV production	0.0151	0.0075	0.0050	0.0038	0.0030	0.0025	0.0013

[1] Based on the datasheet of batteries that match the capacity requirements, from [79].

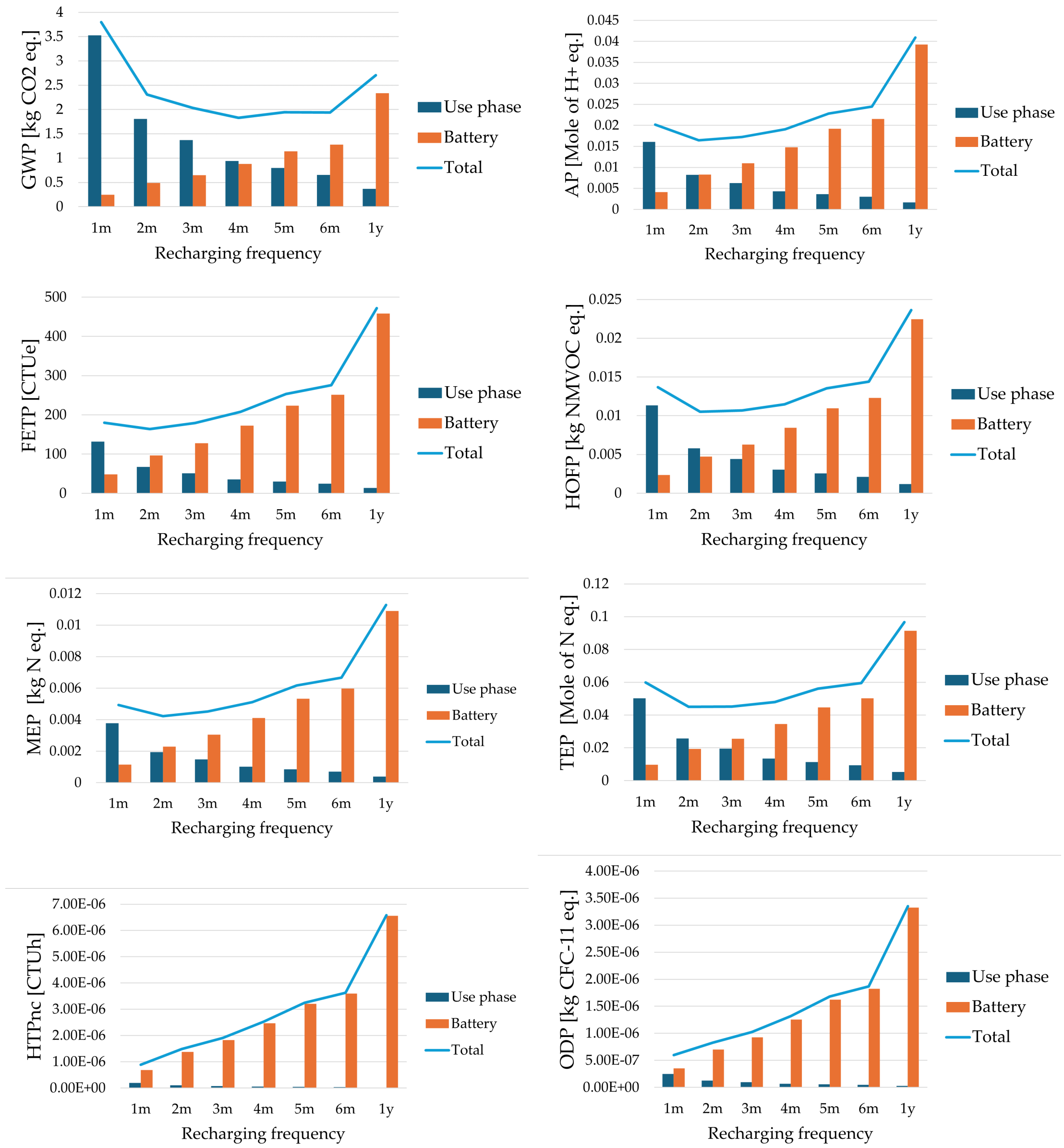

Figure 3.19: Evolution of the LCIA results for the use phase and the production of rechargeable battery in multiple impact categories depending on the recharging frequency, per sensor. The production of the UAV is included in the total, but is much smaller than the other values and is therefore not displayed on the figures as it has no influence on the total.

3.4.2 Influence of the Mode of Transport on the Distribution Phase

In order to understand the influence of the mode of transport used during the distribution phase on the LCIA results, the Solar solution will be used as the reference. Two mode of transport will be evaluated, the truck and the cargo plane. This choice was based on the means used by Dryad when shipping their products.

The distance travelled is the same for the two mode observed, namely 1650 km. The flows taken into consideration are the production of diesel for the truck and paraffin for the plane, as well as their combustion by the two means of transport. First, the influence on the distribution phase alone is observed. Then, the influence on the solution as a whole is studied.

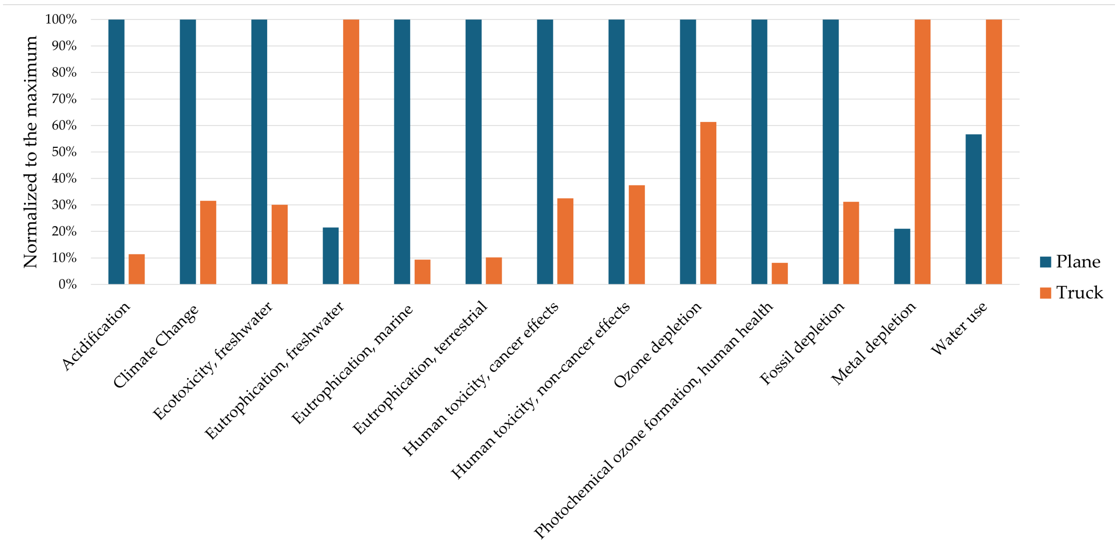

Figure 3.20: LCIA cradle-to-grave results - Influence of the mean of transport on the distribution phase results, normalised in relation to the results for the use of a plane, apart for the freshwater eutrophication, metal depletion and water use, normalised to the use of a truck.

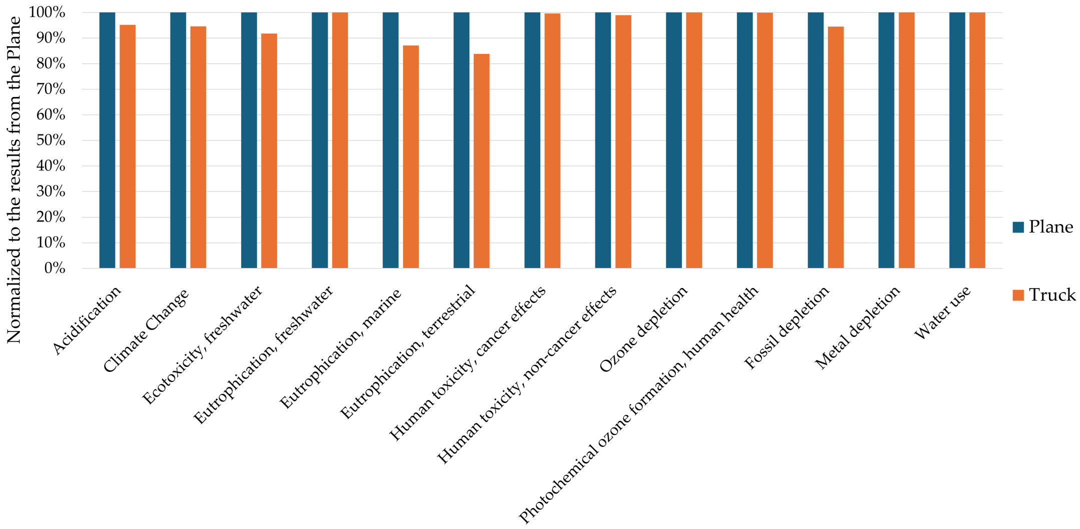

Figure 3.21: LCIA cradle-to-grave results - Influence of the mean of transport on the Solar solution results, normalised to the use of a plane.

After the comparison between the two modes, the influence of the distance travelled is studied. The flows from the database are the same. The first distance is the one used previously, 1650 km, between Auriol and Berlin. The other distance is between Berlin and Ottawa airports, 6150 km according to Google Maps.

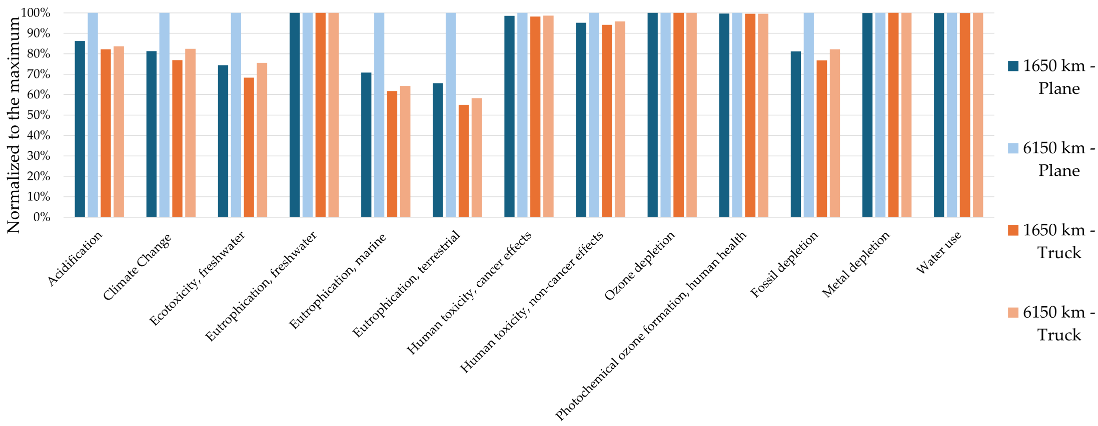

Figure 3.22: LCIA cradle-to-grave results - Influence of the distance travelled with different mode of transport on the Solar solution results, normalised to the distance of 6150 km, with a plane.

3.4.3 Influence of the Manufacturing Location on the Solar Solution

The paper, from which the LCIA results of the solar cells were taken, assumes the location of manufacturing to be Europe. As of today, most of the PV panels are produced in China[67][76] [89]. Fortunately, Galley et al. [60] checked the impact that the change in location had on solar cell production.

Important detail to note, the transport of the solar cells from China to Europe, as the sensors are assembled near Berlin, is not considered here.

Table 3.19: Difference between China and Europe for the production of solar cell, in %, from Galley et al. [60].

	Europe	**China**
Acidification	63%	100%
Climate Change	55%	100%
Ecotoxicity, freshwater	88%	100%
Eutrophication, freshwater	100%	99%
Eutrophication, marine	54%	100%
Eutrophication, terrestrial	57%	100%
Human toxicity, cancer effects	81%	100%
Human toxicity, non-cancer effects	86%	100%
Ozone depletion	100%	90%
Photochemical ozone formation, human health	56%	100%
Fossil depletion	66%	100%
Metal depletion	100%	100%
Water use	47%	100%

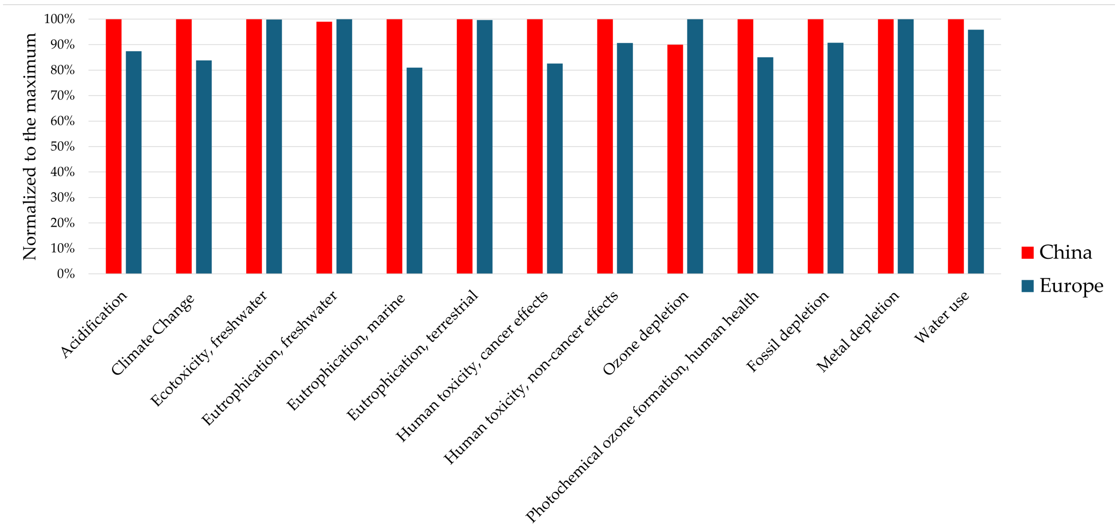

Figure 3.23: LCIA cradle-to-grave results - Influence of the manufacturing location on the Solar solution, per sensor. Normalised to the location in China, apart for the freshwater eutrophication and ozone depletion.

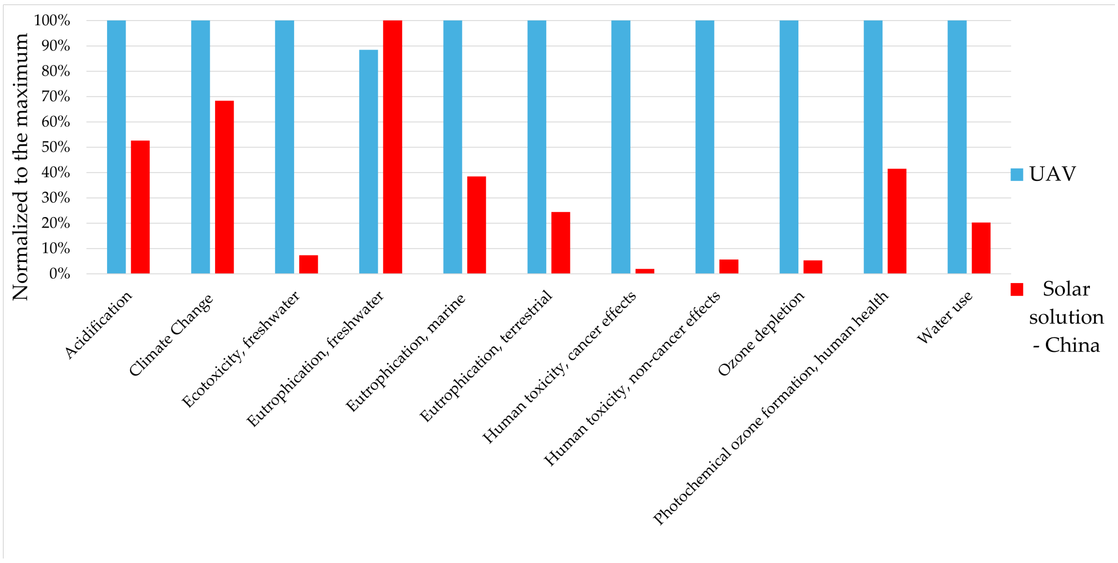

Figure 3.24: LCIA cradle-to-grave results - Comparison between the UAV and Solar solutions with the location set to China, per sensor. Results are normalised to the UAV solution, apart for the freshwater eutrophication to which they are normalised to the Solar solution.

Table 3.20: This table complements Figure 3.24, by also including the Solar solution manufactured in Europe. The LCIA results of the UAV solution in the freshwater eutrophication is 88% of the Solar solution, regardless of the manufacturing location.

	UAV Solution	**Solar solution Europe**	**Solar solution China**
Acidification	100%	46%	53%
Climate Change	100%	57%	68%
Ecotoxicity, freshwater	100%	7%	7%
Eutrophication, marine	100%	31%	38%
Eutrophication, terrestrial	100%	24%	24%
Human toxicity, cancer effects	100%	2%	2%
Human toxicity, non-cancer effects	100%	5%	6%
Ozone depletion	100%	6%	5%
Photochemical ozone formation, human health	100%	35%	41%
Water use	100%	19%	20%

Chapter 4

Discussion

This chapter has three purposes: to interpret the results, to contextualise them and to discuss possible improvements, explore the limitations of this study.

4.1 Interpretation

This is the final stage of an LCA. Its purpose is to link and analyse the results of all the previous phases, while critically reviewing the methodology used so far.

The key messages that can be drawn from the comparison of results for the different energy sources are as follows:

- The Battery solution has a higher impact in all categories, by far, as there is no impact category where the results of another solution are even half of its own. This is due to the production of its battery (Figure 3.17).
- Of the three solutions, the Solar solution has lower impacts in all categories, except for freshwater eutrophication, where the results for the UAV solution are lower. In addition, outside the acidification and climate change categories, the Solar solution has less than 50% of the impact of the UAV solution (Figure 3.18).
- The results for the production of SC are lower in all studied categories compared to the production of lithium battery (Table 3.17).
- The mean of transport has a great influence on the distribution phase but is less impactful on the overall results (Figure 3.20 and 3.21). The distance travelled by truck does not have a high impact, whereas the distance by plane is an important factor (Figure 3.22).

- The PCB has a much bigger impact on the results of the Solar solution compared to the other two solutions, where the PCB has a lower impact than the MCU. This high contribution is due to the large area of the PCB used. Considering the area of PCB required for the other solutions, there is room for an eco-design of this solution (Figure 3.14).

- The freshwater eutrophication, human health, cancer, and the ozone depletion are dominated by the energy sources, regardless of the solution, with a small contribution from the use phase in the UAV solution, related to the car production (Figure 3.12). Also, the production of solar cell seems to be less impactful on the freshwater eutrophication than the production of lithium battery, to the extent that the solar cell is assumed heavier than the battery from the UAV solution (Figure 3.14).

- The casing dimensions do not have a significant impact on the solution (Figure 3.14 and 3.16).

Key messages specific to each solution are summarized below.

Battery Solution:

- The Battery solution is dominated by the production of lithium batteries (Figure 3.13).

Solar Solution:

- The PCB is the largest contributor in most of the Solar solution results, with the solar cell in second place, followed by MCU production. This high contribution is due to the large area of the PCB used. Considering the amount required for the other solutions, there is room for an eco-design of this solution (Figure 3.14).

- The solar cell production has a lower impact than expected in other categories than freshwater eutrophication, human health, both cancer and non-cancer, and ozone depletion. This is partly due to the relatively small size of the solar cell (36 cm^2). But in those four categories, the solar cell production dominates the results of the Solar solution (Figure 3.14).

- The use phase is the second most influential flow in the freshwater ecotoxicity, with more than 20% of the results due to it (Figure 3.14).

- The production of the MCU contributes to around 20% of results for 9 out of 13 impact categories (Figure 3.14).

- The manufacturing location has a high impact on the LCIA results of the production of solar cell, but has a moderate impact on the overall Solar solution. This change becomes even less apparent when compared with the UAV solution. It is not an important factor in the comparison, but it should not be overlooked when deciding where to manufacture the parts (Figure 3.23 and 3.24).

UAV Solution:

- The results of the UAV solution are dominated by the energy source, more precisely the production of lithium batteries, in most impact categories, except for climate change, terrestrial eutrophication and photochemical ozone formation, which are dominated by the use phase. The use phase is the second most influential flow (Figure 3.16).
- The UAV production has no influence on the results of the UAV solution (Figure 3.16).
- The RX coil and its PCB do have a small influence on the results of certain categories. The copper used in the coil is the reason behind the results for the mineral and metal resource depletion. For the rest, the PCB, on which the coil is fixed, is the main source of impact (Figure 3.16).
- For the UAV solution, increasing the recharging frequency has a positive impact on the results of the categories where the use phase is influential (Figure 3.19).
- Rather than being an upper limit, recharging the sensor every two months is close to the optimum recharging frequency, apart from the climate change category, where the optimum is closer to 4 months. All the impact categories where the use phase was the first or second most influential flow, as seen in Figure 3.16, were observed. In addition, the human toxicity, non-cancer, and the ozone depletion, in Figure 3.19, show that the results in categories where the battery is dominant can only be lowered with higher recharging frequencies, an expected outcome as doing such reduces the size of the battery.

4.2 Critical Analysis

This section will look at the results in different perspectives in order to gain a deeper understanding of their significance.

4.2.1 Characterization in Relation to Planetary Boundaries

This section assesses whether the LCIA results remain within globally sustainable limits, offering a critical perspective on the system's sustainability, through a comparison with the planetary boundaries (PB)[90]. The comparison is based on the coverage of the whole forest with 20,160 sensors, rather than being confined to a single functional unit. This broader reference point enables a more comprehensive evaluation of the system's environmental performance.

The category values for the PB are taken from the paper by Sala et al. [91], which were calculated using the ILCD method.

Table 4.1: Proportion of Solar Solution LCIA Results relative to PB, calculated for each impact category with an available planetary boundary score. The reference is the coverage of the entire Parc with 20,160 sensors, rather than the functional unit.

ILCD Impact Category	Units	PB	LCIA results	Ratio of LCIA results to PB
Acidification	mole H+ eq	9.99×10^{11}	2.02×10^{2}	2.1×10^{-10}
Climate change	kg CO_2 eq	6.79×10^{12}	3.89×10^{4}	5.73×10^{-9}
Ecotoxicity freshwater	CTUe	1.31×10^{14}	2.57×10^{5}	1.96×10^{-9}
Freshwater eutrophication	kg P eq	5.79×10^{9}	84.7	1.46×10^{-8}
Marine eutrophication	kg N eq	2.00×10^{11}	31.9	1.60×10^{-10}
Terrestrial eutrophication	mole N eq	6.12×10^{12}	2.65×10^{2}	4.33×10^{-11}
Human toxicity, cancer effects	CTUh	9.16×10^{4}	1.23×10^{-4}	1.34×10^{-9}
Human toxicity, non-cancer effects	CTUh	1.13×10^{6}	1.56×10^{-3}	1.38×10^{-9}
Ozone depletion potential	kg CFC-11 eq	5.38×10^{8}	9.89×10^{-4}	1.84×10^{-12}
Photochemical ozone formation	kg NMVOC eq	2.62×10^{10}	92.9	3.54×10^{-9}
Water depletion	m^3 water eq	6.85×10^{11}	7.14×10^{3}	1.04×10^{-8}

The proportion of the solar solution LCIA results is much smaller than the planetary boundaries.
Another approach would be to allocate the LCIA results to the population. This choice is arbitrary, results normalised in relation to planetary limits vary according to the allocation key used.

The study case is located in the Var department, which had a population of 1 095 337 in 2021 [92]. To obtain the planetary boundaries per capita, it is necessary to divide the values from Table 4.1 with the world population in 2021, i.e., 7 954 448 391 [93]. Using the data from 2021 is a lower bound as the world population is continuously increasing and the PB per capita would only decrease in the future. The proportion are given in the following table.

Table 4.2: Proportion of Solar Solution LCIA Results Relative to Planetary Boundaries, per Capita, calculated for each impact category with an available planetary boundary score. The reference is the coverage of the entire Parc with 20,160 sensors, rather than the functional unit.

ILCD Impact Category	Units	Proportion of the PB, per capita [%]
Acidification	mole H+ eq	0.00015
Climate change	kg CO_2 eq	0.00416
Ecotoxicity freshwater	CTUe	0.00143
Freshwater eutrophication	kg P eq	0.01062
Marine eutrophication	kg N eq	0.00012
Terrestrial eutrophication	mole N eq	0.00003
Human toxicity, cancer effects	CTUh	0.00097
Human toxicity, non-cancer effects	CTUh	0.001
Ozone depletion potential	kg CFC-11 eq	0.00000
Photochemical ozone formation	kg NMVOC eq	0.00257
Water depletion	m^3 water eq	0.00757

In both approaches, it seems that the LCIA results of the Solar solution are acceptable in a broader perspective.

Now for the comparison of the three. The coverage of the total forest area worldwide, i.e., 4.05 billion hectares [94] is assumed for this comparison, requiring 972 millions sensors at a rate of 0.24 sensor/ha. This number might seem disproportionate but represents only 6.11 % of the total amount of IoT devices in the world in 2021, i.e. 15.9 billions [6].

Table 4.3: Proportion of the three solution LCIA results relative to Planetary boundaries, with the coverage of the total forest area worldwide as reference.

ILCD Impact Category	Solar solution [%]	Battery solution [%]	UAV solution [%]
Acidification	0.001	0.010	0.002
Climate change	0.029	0.094	0.051
Freshwater ecotoxicity	0.010	0.847	0.135
Freshwater eutrophication	0.074	0.715	0.065
Freshwater eutrophication	0.001	0.013	0.003
Terrestrial eutrophication	0.000	0.004	0.001
Human toxicity, cancer effects	0.007	4.721	0.424
Human toxicity, non-cancer effects	0.007	1.395	0.135
Ozone depletion potential	0.000	0.001	0.000
Photochemical ozone formation	0.018	0.213	0.051
Water depletion	0.053	2.388	0.270

This new perspective reveals that the impact of the solar solution is acceptable when considered in the context of the global scale. However, it also indicates that the battery solution should be avoided, while the UAV solution might require some changes to be acceptable.

4.2.2 Contextualizing Results within Forest Fire Emissions

Following the comparison with the planetary boundaries, this section compares the with the context of the solution, i.e. forest fires.

As explained in the section 1.1, the emissions from a forest fire depend on many factors. From the biome to the amount of fuel available, it varies in intensity, therefore the amount of particulate matter and greenhouse gas changes. As this study takes place in a Mediterranean forest, this biome will be chosen. If a forest fire in the Mediterranean biome were to start, 1 ha of burnt forest emits 61.38×10^3 [kgCO_2eq] on average [21]. Covering the surroundings of one km of road, or 400 ha of forest, with the sensors results in the emission of 154 kgCO_2eq. Covering the whole "Parc naturel régional de la Sainte-Baume" would require the production of 20160 sensors and result in the emission of 38.9×10^3 kgCO_2eq. On the greenhouse gas emissions,

4.2.3 Lithium Batteries as a Potential Fire Source

While this thesis focuses on the environmental impact of energy sources, it is essential to maintain a clear and critical perspective on the work itself. The purpose of the IoT sensor network in this special case is to prevent fire propagation.

Regardless of the environmental results, the problem of flammability in lithium batteries raises questions [95].

A lithium battery can malfunction and become a source of fire. This is relatively rare, but it has happened in the past [96]. In this particular case, the possible causes of ignition would be overcharging, with the UAV solution, or extreme moisture [95], but both are unlikely to happen.
However, a lithium battery can catch fire. If a fire breaks out near a sensor, there are two possibilities: the sensor informs its owner of the fire and the owner reacts quickly enough to extinguish it; the sensor informs its owner, but in the meantime it catches fire and becomes a source of fire. Extinguishing a lithium battery that caught fire is not an easy feat. Indeed, the class of such fire is B, like cooking oil, meaning that using water is not a good solution when fighting against it, as it tends to spread the flames [97][98].

Although unlikely, the risk of fire does exist. It is therefore important to ensure that the solution does not inadvertently become the problem. An IoT network designer should bear this in mind when designing a solution in this context.

In light of the above, the critical review of the results can be resumed.

4.2.4 Future Improvements per Solution

UAV Solution

The use phase appears to be the hot spot in the UAV solution, dominated by the distance travelled by car when the recharging frequency is high, by the battery production when it is low.

One way to drastically reduce the impact of the UAV solution would be to stop using diesel-powered cars. Using an electric car could be a solution. For some impact categories, such as climate change, this would be true, but not for others, such as acidification, human toxicity, particulate matter, photochemical ozone creation and resource depletion, for which the use of electric-powered vehicle would mean greater impacts [99]. So the solution may be not to use cars at all. An idea would be to install charging stations for UAV in range of sensors, with solar panels or connected to the grid, while charging the sensors at a much higher rate, to increase the range of the UAVs, as they would need to transport less weight. Or to limit the use of this solution to places close to buildings or in buildings. For example, in a warehouse, where no other energy source is available and pulling a cable would be too costly.

With a charging frequency of one week, one UAV can service 15.37 sensors for 10 years. A sensor needs 50.5 mAh, or 436 J, to last a week. The only contribution to the use phase is an electricity production of approximately 4.23 [MJ] over the lifetime of the sensor, based on Equation 3.5. The climate change impact is of 0.107 [kg$C0_2$eq] for the UAV production, 0.088 [kg$C0_2$eq] for the lithium battery of 3g [79] production and 0.280 [kg$C0_2$eq] for the electricity production. And for the metal depletion, a relevant category to look into, the production of UAV amount $4.30 \times 10^{-}3$ [kg Cu eq.], $3.77 \times 10^{-}5$ [kg Cu eq.] for the lithium battery and insignificant for the electricity. In comparison, with the assumption that 1m of $\varnothing$mm copper wire weighs 28.16g, the production of copper wire is equivalent to 0.11 [kg $C0_2$ eq] and 0.0425 [kg Cu eq.] per meter of cable. If a cable longer than 4.32 m is necessary to the deployment, the UAV solution appears to be a better choice. This result should be taken with caution, as many parameters have been left out, such as electricity production in the case of copper wire. It is there to show a potential application for the UAV solution, but in no way proves that it would actually be a better solution.

The UAV solution has potential, but is constrained by the range of its UAV. The benefits it can bring to society will depend on its implementation and the way in which it is used.

Solar Solution

The area of PCB used has a significant effect on the results of the Solar solution. The reason for this large surface area is that the entire solar panel is attached to the PCB, as well as the two SCs. As the impact of the casing are negligible, an idea of improvement would be to redesign the casing so that the panel could be detached from the PCB and connected to the PCB using wires, and do the same with the SCs. This would reduce the surface area of PCBs used and, at the same time, most of the environmental impact of the solution.

Battery Solution

Unfortunately, an eco-design of this solution seems hard to find, as the only contributor to its results is the battery. There is still room for improvement, related to the consumption of the sensor. Indeed, if the IoT node were to consume less power, smaller batteries would be needed. But this has more to do with the design of the node than that of the energy source.

Conclusion

Forest fires have a clear impact not only on the ecosystem but also on the economy and health of the human society, and fighting against them is primordial. Through control, prevention and suppression, there are several strings to a government's bow to prevent massive outburst of fire and therefore massive CO_2 emissions. IoT sensor networks are entirely legitimate in this fight and can be of great help in the control and suppression of forest fires, thanks to their continuous monitoring and fast detection system.

This master thesis is part of the never-ending quest for progress by approaching the development of the solution with a critical eye, so that it does not become worse than the problem it is trying to solve.

To accomplish this, a comparative LCA was performed on an IoT network of 80 sensors, taking the energy supply strategy as point of comparison. Three were considered, a solar cell, harvesting and storing the solar energy in a supercapacitor, a battery, designed to last ten years, and a rechargeable battery, recharged every two months by a UAV via wireless power transfer.

Several impact categories were taken into account to determine whether one of these solutions outweighed the others, or whether one of them stood out positively, to cover the surface of one kilometre of road. This required the production of 80 sensors.

As a result, harvesting solar energy using a solar cell is less damaging to the environment, especially as the production of lithium batteries has a significant impact on many aspects of the ecosystem. For the most commonly used impact category, GWP, the three solutions gave the following results 154 [kgCO_2eq] for the solar harvesting option, 504 [kgCO_2eq] for the battery and 270 [kgCO_2eq] for UAV recharging.

In other categories, the battery solution has significantly higher environmental impacts than the solar and UAV solutions. For the acidification potential, the battery solution's impact is almost ten times greater than the solar solution and four times greater than the UAV solution. The disparity is even more pronounced for freshwater ecotoxicity, where the impact of the battery solution reaches 8.72×10^4 CTUe, compared to only 1.02×10^3 CTUe for the solar solution and $1.39 \times$

10^4 CTUe for the drone, and human toxicity, both cancerous and non-cancerous, with the battery impact being 1,000 times greater than that of the solar solution and 100 times greater than that of the UAV.

In addition, the water consumption for the battery solution is 1.29×10^3 m^3 of water eq., much higher than the solar solution (28.32) and the drone solution (146.0).

This comparative LCA shows that the solar solution offers a less damaging alternative, with significantly lower environmental impacts than its competitors.

Concerning the UAV solution, the door to its development should not be closed, as its main issue was the use phase. Its range of a few kilometres at best makes it difficult to integrate into a network of several kilometres. But it could find a place in smaller systems.

Two other points in favour of the UAV and solar solution are, on the one hand, that the service life in this study was set at 10 years, but both solutions could last longer without changing their design, while the battery solution would either need a larger battery or require a battery change. On the other hand, they both have room for eco-design.

However, these results are certainly an incomplete picture of reality. The quality of the data is far from perfect, in particular because of the different sources used to model the different parts of the solutions. For a more accurate analysis of the results, one way of improving them would be to carry out an uncertainty analysis on the different production processes.

Three impact categories were left out during this LCA, the land use, the ionizing radiation, human health, and the particulate matter emissions, due to lack of data from the reference used in for the Solar solution.

In future work, it would be interesting to develop EoL of solar cells. It would also be worthwhile to develop the use phase of the UVA solution.

Appendix A

LCI Model

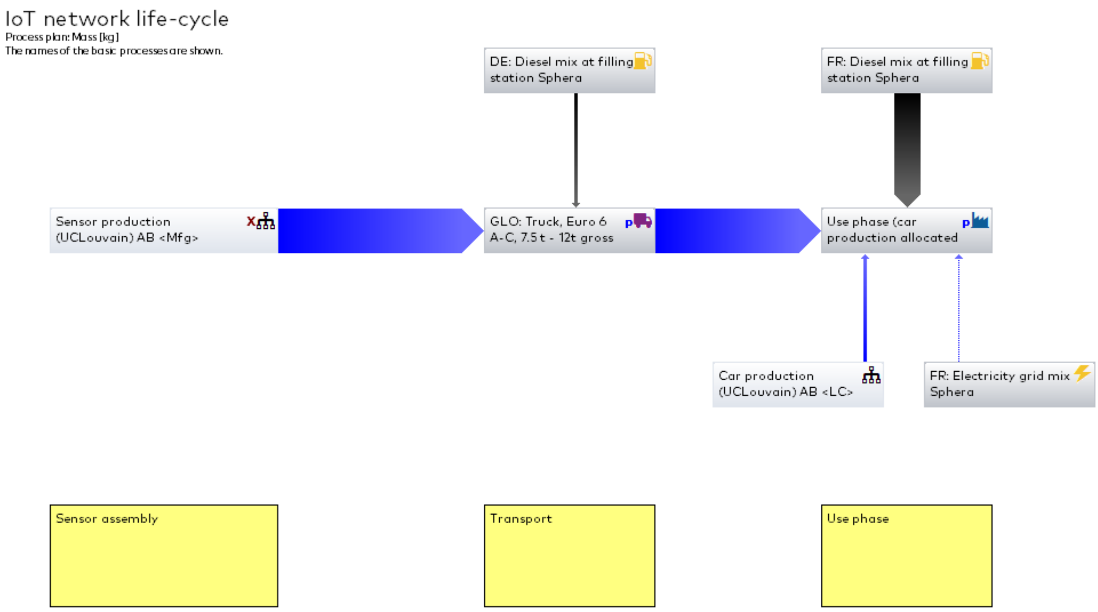

Figure A.1: IoT network life-cycle.

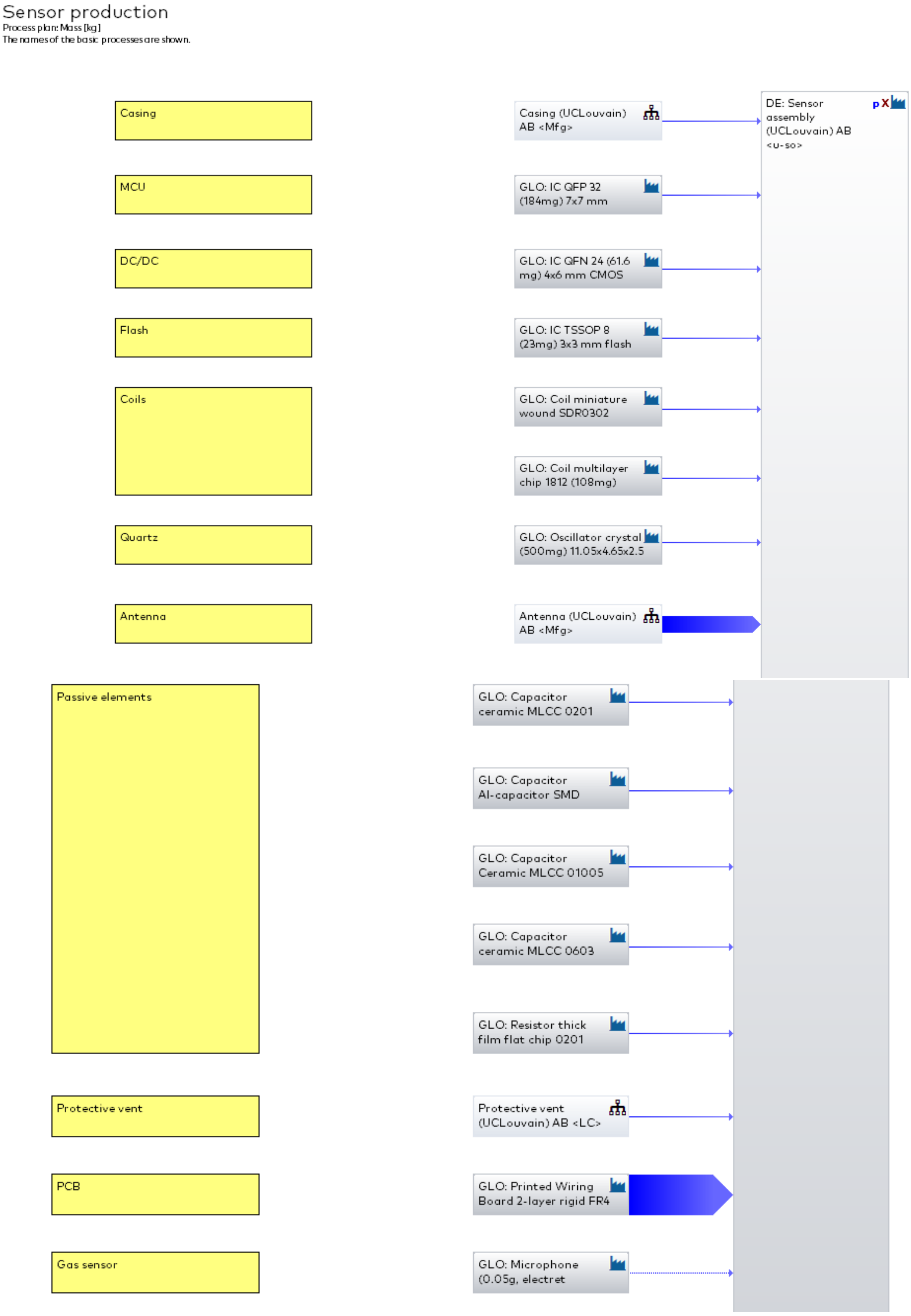

Figure A.2: Sensor production (1/2)

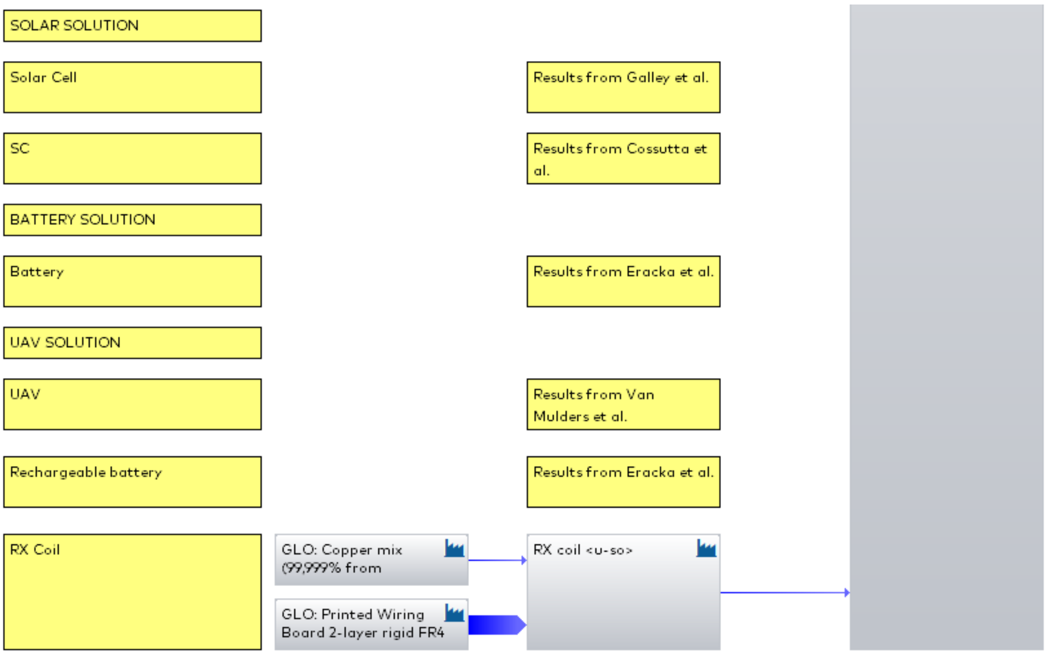

Figure A.3: Sensor production (2/2).

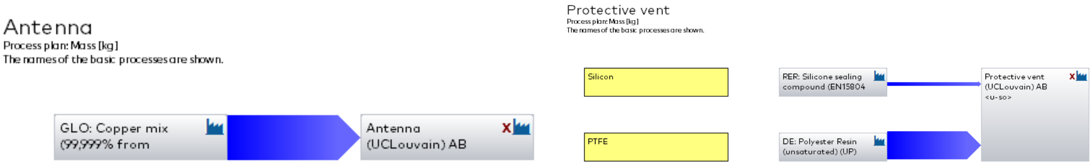

Figure A.4: Left: Antenna. Right: Protective Vent.

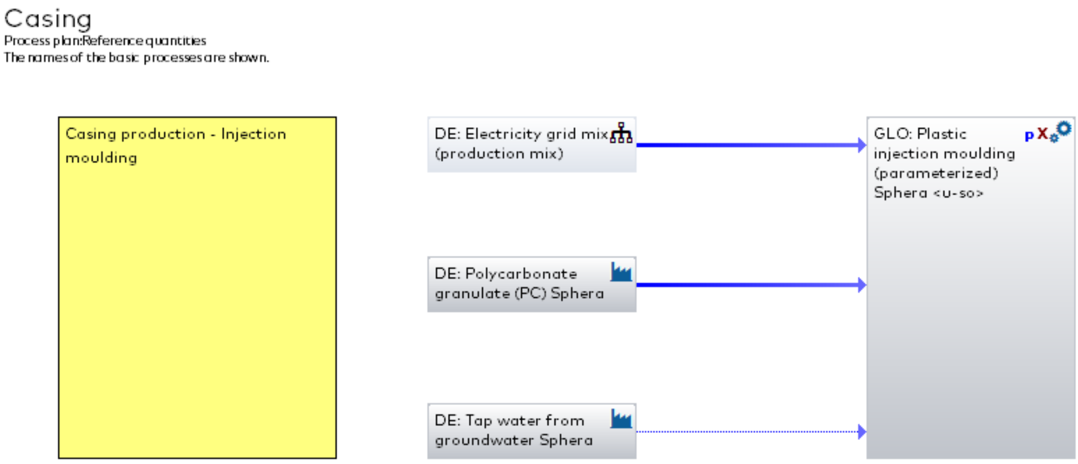

Figure A.5: Casing production.

Appendix B

Impact Categories

Table B.1: Overview of the ILCD impact categories from [100]. (1/2)

Impact Category / Indicator	Unit	Description
Climate change – total, fossil, biogenic, and land use	kg CO2-eq	Indicator of potential global warming due to emissions of greenhouse gases to the air. Divided into 3 subcategories based on the emission source: (1) fossil resources, (2) bio-based resources, and (3) land use change.
Ozone depletion	kg CFC-11-eq	Indicator of emissions to air that causes the destruction of the stratospheric ozone layer
Acidification	kg mol H+	Indicator of the potential acidification of soils and water due to the release of gases such as nitrogen oxides and sulfur oxides
Eutrophication – freshwater	kg PO4-eq	Indicator of the enrichment of the freshwater ecosystem with nutritional elements, due to the emission of nitrogen or phosphor-containing compounds
Eutrophication – marine	Kg N-eq	Indicator of the enrichment of the marine ecosystem with nutritional elements, due to the emission of nitrogen-containing compounds.

Table B.2: Overview of the ILCD impact categories from [100]. (2/2)

Impact Category / Indicator	Unit	Description
Eutrophication – terrestrial	mol N-eq	Indicator of the enrichment of the terrestrial ecosystem with nutritional elements, due to the emission of nitrogen-containing compounds.
Photochemical ozone formation	kg NMVOC-eq	Indicator of emissions of gases that affect the creation of photochemical ozone in the lower atmosphere (smog) catalyzed by sunlight.
Depletion of abiotic resources – minerals and metals	kg Sb-eq	Indicator of the depletion of natural non-fossil resources.
Depletion of abiotic resources – fossil fuels	MJ, net calorific value	Indicator of the depletion of natural fossil fuel resources.
Human toxicity – cancer, non-cancer	CTUh	Impact on humans of toxic substances emitted to the environment. Divided into non-cancer and cancer-related toxic substances.
Eco-toxicity (freshwater)	CTUe	Impact on freshwater organisms of toxic substances emitted to the environment.
Water use	m3 world eq. deprived	Indicator of the relative amount of water used, based on regionalized water scarcity factors.
Land use	Dimensionless	Measure of the changes in soil quality (Biotic production, Erosion resistance, Mechanical filtration).
Ionizing radiation, human health	kBq U-235	Damage to human health and ecosystems linked to the emissions of radionuclides.
Particulate matter emissions	Disease incidence	Indicator of the potential incidence of disease due to particulate matter emissions

Bibliography

[1] © Cambridge University Press. *petrichor*. URL: https://dictionary.cambridge.org/dictionary/english/petrichor. (Accessed April 2, 2024).

[2] Jeffrey Kane. "forest fire". In: *Encyclopedia Britannica* (2024). URL: https://www.britannica.com/science/forest-fire. (accessed June 18, 2024).

[3] Juliette Biao Koudenoukpo. "As Wildfires Increase, Integrated Strategies for Forests, Climate and Sustainability Are Ever More Urgent". In: *UN Chronicle* (31 July 2023). URL: https://www.un.org/en/un-chronicle/wildfires-increase-integrated-strategies-forests-climate-and-sustainability-are-ever-0. (Accessed April 27, 2024).

[4] U.S. Congress Joint Economic Committee. *Climate-Exacerbated Wildfires Cost As Much as* $893 Billion Per Year Top-end Annual Total Costs and Losses (Billions)$*.* URL: https://www.jec.senate.gov/public/_cache/files/9220abde-7b60-4d05-ba0a-8cc20df44c7d/jec-report-on-total-costs-of-wildfires.pdf. (Accessed August 8, 2024).

[5] Dryad Networks GmbH. *Connecting the natural world*. URL: https://www.dryad.net. (Accessed April 5, 2024).

[6] Statista. *Number of Internet of Things (IoT) connections worldwide from 2022 to 2023, with forecasts from 2024 to 2033*. URL: https://www.statista.com/statistics/1183457/iot-connected-devices-worldwide/. (Accessed March 17, 2024).

[7] Marco Gonzalez et al. "Technical and Ecological Limits of 2.45-GHz Wireless Power Transfer for Battery-Less Sensors". In: *IEEE Internet of Things Journal* 10 (17 Sept. 2023), pp. 15431–15442. ISSN: 23274662. DOI: 10.1109/JIOT.2023.3263976.

[8] J. MacCarthy et al. "The Latest Data Confirms: Forest Fires Are Getting Worse". In: *World Resources Institute* (29 August 2023). URL: https://www.wri.org/insights/global-trends-forest-fires. (accessed June 19, 2024).

[9] Francesca Di Giuseppe et al. "Global seasonal prediction of fire danger". In: *Scientific Data* 11 (1 Dec. 2024). ISSN: 20524463. DOI: 10.1038/s41597-024-02948-3.

[10] National Geographic. *Wildfires: How They Form, and Why They're so Dangerous*. URL: https://education.nationalgeographic.org/resource/wildfires-how-they-form-and-why-theyre-so-dangerous/. (Accessed June 19, 2024).

[11] Colin G. Price. "Lightning Applications in Weather and Climate Research". In: *Surveys in Geophysics* 34 (6 Nov. 2013), pp. 755–767. ISSN: 01693298. DOI: 10.1007/s10712-012-9218-7.

[12] European Environment Agency (EEA). *11.B Forest fires 2023*. 6Oct 2023. URL: https://www.eea.europa.eu/publications/emep-eea-guidebook-2023.

[13] Joe H Scott, Matthew P Thompson, and David E Calkin. *A Wildfire Risk Assessment Framework for Land and Resource Management*. 2013. URL: http://www.fs.fed.us/rmrs.

[14] Wikipedia. *Pinus contorta*. URL: https://en.wikipedia.org/wiki/Pinus_contorta. (Accessed August 8, 2024).

[15] WFCA. *Effects of Wildfires on the Environment*. URL: https://wfca.com/wildfire-articles/effects-of-wildfires-on-the-environment/. (Accessed August 8, 2024).

[16] National Geographic. *The Ecological Benefits of Fire*. URL: https://education.nationalgeographic.org/resource/ecological-benefits-fire/. (Accessed August 8, 2024).

[17] Emilio Chuvieco. *Earth observation of wildland fires in mediterranean ecosystems*. Springer Berlin Heidelberg, 2009, pp. 1–257. ISBN: 9783642017537. DOI: 10.1007/978-3-642-01754-4.

[18] Drew Martin, Mai Tomida, and Brian Meacham. "Environmental impact of fire". In: *Fire Science Reviews* 5 (1 Dec. 2016), p. 5. ISSN: 2193-0414. DOI: 10.1186/s40038-016-0014-1. URL: http://firesciencereviews.springeropen.com/articles/10.1186/s40038-016-0014-1.

[19] EPA. *Why Wildfire Smoke is a Health Concern*. URL: https://www.epa.gov/wildfire-smoke-course/why-wildfire-smoke-health-concern. (Accessed August 16, 2024).

[20] Carlos et al. "Forest Fire Emissions and Air Pollution in Southern Europe". In: ed. by Emilio Chuvieco. Springer Berlin Heidelberg, 2009, pp. 171–187. ISBN: 978-3-642-01754-4. DOI: 10.1007/978-3-642-01754-4_12. URL: https://doi.org/10.1007/978-3-642-01754-4_12.

[21] Carla Scarpa et al. "Estimating annual GHG and particulate matter emissions from rural and forest fires based on an integrated modelling approach". In: *Science of the Total Environment* 907 (Jan. 2024). ISSN: 18791026. DOI: 10.1016/j.scitotenv.2023.167960.

[22] Evgenii Ponomarev et al. "Current Trend of Carbon Emissions from Wildfires in Siberia". In: *Atmosphere* 12 (5 2021). ISSN: 2073-4433. DOI: 10.3390/atmos12050559. URL: https://www.mdpi.com/2073-4433/12/5/559.

[23] Sarah Farmer and Jenni Moore Myers. *Economic risks: Forest Service estimates costs of fighting wildfires in a hotter future*. URL: https://www.fs.usda.gov/about-agency/features/economic-risks-forest-service-estimates-costs-fighting-wildfires-hotter. (Accessed August 8, 2024).

[24] Carlyn J. Matz et al. "Health impact analysis of PM2.5 from wildfire smoke in Canada (2013–2015, 2017–2018)". In: *Science of the Total Environment* 725 (July 2020). ISSN: 18791026. DOI: 10.1016/j.scitotenv.2020.138506.

[25] WHO. *Wildfires*. URL: https://www.who.int/health-topics/wildfires/#tab=tab_1. (Accessed August 16, 2024).

[26] Gabrielle Denault. *The impact of forest fires on human health*. URL: https://observatoireprevention.org/en/2021/08/31/the-impact-of-forest-fires-on-human-health/. accessed August 16, 2024.

[27] EPA. *Wildland Fire Research: Health Effects Research*. URL: https://www.epa.gov/air-research/wildland-fire-research-health-effects-research. (Accessed August 16, 2024).

[28] Carolyn Black et al. *Wildfire smoke exposure and human health: Significant gaps in research for a growing public health issue*. Oct. 2017. DOI: 10.1016/j.etap.2017.08.022.

[29] Naseem S. Miller. "Wildfires have long-term health effects, both direct and indirect, several studies show". In: *The Journalist's Resource* (July 26, 2023). (Accessed August 16, 2024).

[30] Nicolò Camarretta et al. *Monitoring forest structure to guide adaptive management of forest restoration: a review of remote sensing approaches*. July 2020. DOI: 10.1007/s11056-019-09754-5.

[31] Swagata Payra, Ajay Sharma, and Sunita Verma. "Chapter 14 - Application of remote sensing to study forest fires". In: ed. by Abhay Kumar Singh and Shani Tiwari. Elsevier, 2023, pp. 239–260. ISBN: 978-0-323-99262-6. DOI: https://doi.org/10.1016/B978-0-323-99262-6.00015-8. URL: https://www.sciencedirect.com/science/article/pii/B9780323992626000158.

[32] NASA. *MODIS Moderate Resolution Imaging Spectroradiometer*. URL: https://modis.gsfc.nasa.gov/. (Accessed March 17, 2024).

[33] Francesco Carta et al. *Advancements in Forest Fire Prevention: A Comprehensive Survey*. July 2023. DOI: 10.3390/s23146635.

[34] Gilles Callebaut et al. "The art of designing remote iot devices—technologies and strategies for a long battery life". In: *Sensors (Switzerland)* 21 (3 Feb. 2021), pp. 1–37. ISSN: 14248220. DOI: 10.3390/s21030913.

[35] Matteo Cerchecci et al. "A low power IoT sensor node architecture for waste management within smart cities context". In: *Sensors (Switzerland)* 18 (4 Apr. 2018). ISSN: 14248220. DOI: 10.3390/s18041282.

[36] Team Celona. *IoT Architecture: Complete Explanation with Examples*. URL: https://www.celona.io/network-architecture/iot-architecture. (Accessed March 17, 2024).

[37] GeeksforGeeks. *Sensors in Internet of Things(IoT)*. URL: https://www.geeksforgeeks.org/sensors-in-internet-of-thingsiot/. (Accessed August 18, 2024).

[38] Pooja Choudhary et al. "A survey - Energy harvesting sources and techniques for internet of things devices". In: *Materials Today: Proceedings*. Vol. 30. Elsevier Ltd, 2020, pp. 52–56. DOI: 10.1016/j.matpr.2020.04.115.

[39] Wikipedia. *Solar cell*. URL: https://en.wikipedia.org/wiki/Solar_cell. (Accessed August 18, 2024).

[40] Emmanuel De Jaeger. *LENVI2007 - Renewable Energy Sources - Photovoltaic Systems*. (Accessed June 29, 2024).

[41] IEA. *Photovoltaics Report-Fraunhofer Institute for Solar Energy Systems, ISE with the support of PSE Projects GmbH*. 2024. URL: www.ise.fraunhofer.de. (Accessed August 15, 2024).

[42] Wikipedia. *Czochralski method*. URL: https://en.wikipedia.org/wiki/Czochralski_method. (Accessed August 18, 2024).

[43] SinoVoltaics Niclas. *Solar Cell Production: from silicon wafer to cell*. URL: https://sinovoltaics.com/solar-basics/solar-cell-production-from-silicon-wafer-to-cell/. (Accessed August 16, 2024).

[44] Antti Väyrynen and Justin Salminen. "Lithium ion battery production". In: *Journal of Chemical Thermodynamics* 46 (Mar. 2012), pp. 80–85. ISSN: 00219614. DOI: 10.1016/j.jct.2011.09.005.

[45] Wikipedia. *Lithium-ion battery.* URL: https://en.wikipedia.org/wiki/Lithium-ion_battery. (Accessed July 24, 2024).

[46] SinoVoltaics Niclas. *Energy Density and Specific Energy of Battery.* URL: https://sinovoltaics.com/learning-center/storage/energy-density-and-specific-energy-of-battery/. (Accessed August 18, 2024).

[47] Wendy Pantoja, Jaime Andres Perez-Taborda, and Alba Avila. *Tug-of-War in the Selection of Materials for Battery Technologies.* Sept. 2022. DOI: 10.3390/batteries8090105.

[48] Jarne Van Mulders et al. "UAV-based solution for extending the lifetime of IoT devices: efficiency, design and sustainability". In: *Frontiers in Communications and Networks* 5 (2024). ISSN: 2673530X. DOI: 10.3389/frcmn.2024.1341081.

[49] Wikipedia. *Wireless power transfer.* URL: https://en.wikipedia.org/wiki/Wireless_power_transfer. (Accessed August 18, 2024).

[50] Pol Maistriaux et al. "Modeling the Carbon Footprint of Battery-Powered IoT Sensor Nodes for Environmental-Monitoring Applications". In: Association for Computing Machinery, Nov. 2022, pp. 9–16. ISBN: 9781450396653. DOI: 10.1145/3567445.3567448.

[51] Michael Z Hauschild, Ralph K Rosenbaum, and Stig Irving Olsen. *Life Cycle Assessment.* 2018.

[52] Patricia Luis. *LEPL1804 Développement durable et transition Life cycle assessment (LCA) Life cycle assessment.* (Accessed June 29, 2024).

[53] Dryad Networks GmbH. *Dryad Silvanet Documentation.* URL: https://docs.dryad.app/. (Accessed April 5, 2024).

[54] Bosch. *Gas Sensor BME688.* URL: https://www.bosch-sensortec.com/products/environmental-sensors/gas-sensors/bme688/. (Accessed July 28, 2024).

[55] Thibault Pirson and David Bol. "Assessing the embodied carbon footprint of IoT edge devices with a bottom-up life-cycle approach". In: *Journal of Cleaner Production* 322 (Nov. 2021). ISSN: 09596526. DOI: 10.1016/j.jclepro.2021.128966.

[56] Jarne Van Mulders et al. "UAV-Based Servicing of IoT Nodes: Assessment of Ecological Impact". In: *Sensors* 23 (4 Feb. 2023). ISSN: 14248220. DOI: 10.3390/s23042291.

[57] Inc. Sphera Solutions. *Product Life Cycle Assessment Solutions*. URL: https://sphera.com/solutions/product-stewardship/life-cycle-assessment-software-and-data/. (Accessed March 8, 2024).

[58] Matteo Cossutta et al. "A comparative life cycle assessment of graphene and activated carbon in a supercapacitor application". In: *Journal of Cleaner Production* 242 (Jan. 2020). ISSN: 09596526. DOI: 10.1016/j.jclepro.2019.118468.

[59] Merve Erakca et al. "Closing gaps in LCA of lithium-ion batteries: LCA of lab-scale cell production with new primary data". In: *Journal of Cleaner Production* 384 (Jan. 2023). ISSN: 09596526. DOI: 10.1016/j.jclepro.2022.135510.

[60] Saori Galley et al. *Double side contacted cells with innovative carrier-selective contacts Deliverable 5.4-Report on environmental LCA*. URL: https://cordis.europa.eu/project/id/727529.

[61] Ducab Metals LLC. URL: https://dmb.ae/uploads/DMB_Can-Weld_Wire_January2020.pdf. (Accessed March 18, 2024).

[62] Wikipedia. *Copper*. URL: https://en.wikipedia.org/wiki/Copper. (Accessed March 15, 2024).

[63] Wikipedia. *Tin*. URL: https://en.wikipedia.org/wiki/Tin. (Accessed March 15, 2024).

[64] Wikipedia. *Injection moulding*. URL: https://en.wikipedia.org/wiki/Injection_moulding. (Accessed July 29, 2024).

[65] Laurent Delannay and Aude Simar. *Lecture slide, UCLouvain LMECA1451 Fabrication mécanique*. 2021.

[66] Dassault Systèmes - SolidWorks Corporation. *Solidworks*. URL: https://www.solidworks.com/.

[67] IEA. *Solar PV*. 2024. URL: https://www.iea.org/energy-system/renewables/solar-pv. (Accessed August 15, 2024).

[68] Trina Solar Science Technology (Thailand) Ltd. *ENVIRONMENTAL PRODUCT DECLARATION - TSM-DE15M(II) and TSM-DE17M(II)*. 2020. URL: https://www.epditaly.it/wp-content/uploads/2016/12/MR-102.1_Trina-Solar_EPDTSM-DE15M-II_TSM-DE17M-II-0PV-Backsheet-Panels.pdf.

[69] LTD RISEN ENERGY CO. *ENVIRONMENTAL PRODUCT DECLARATION - RSM110-8-xxxM and RSM120-8-xxxM*. 2022. URL: https://api.environdec.com/api/v1/EPDLibrary/Files/74e9fbb8-f34a-443e-abaa-08d9c4927501/Data.

[70] Jinglan Hong et al. “Life cycle assessment of multicrystalline silicon photovoltaic cell production in China”. In: *Solar Energy* 133 (Aug. 2016), pp. 283–293. ISSN: 0038092X. DOI: 10.1016/j.solener.2016.04.013.

[71] Peishi Wu et al. “Review on Life Cycle Assessment of Greenhouse Gas Emission Profit of Solar Photovoltaic Systems”. In: *Energy Procedia*. Vol. 105. Elsevier Ltd, 2017, pp. 1289–1294. DOI: 10.1016/j.egypro.2017.03.460.

[72] Laurence Stamford and Adisa Azapagic. “Environmental Impacts of Photovoltaics: The Effects of Technological Improvements and Transfer of Manufacturing from Europe to China”. In: *Energy Technology* 6 (6 June 2018), pp. 1148–1160. ISSN: 21944296. DOI: 10.1002/ente.201800037.

[73] Amelie Müller et al. “A comparative life cycle assessment of silicon PV modules: Impact of module design, manufacturing location and inventory”. In: *Solar Energy Materials and Solar Cells* 230 (Sept. 2021). ISSN: 09270248. DOI: 10.1016/j.solmat.2021.111277.

[74] Vasilis Fthenakis and Enrica Leccisi. “Updated sustainability status of crystalline silicon-based photovoltaic systems: Life-cycle energy and environmental impact reduction trends”. In: *Progress in Photovoltaics: Research and Applications* 29 (10 Oct. 2021), pp. 1068–1077. ISSN: 1099159X. DOI: 10.1002/pip.3441.

[75] Ehsan Alam and Xiaohong Xu. “Life cycle assessment of photovoltaic electricity production by mono-crystalline solar systems: a case study in Canada”. In: *Environmental Science and Pollution Research* 30 (10 Feb. 2023), pp. 27422–27440. ISSN: 16147499. DOI: 10.1007/s11356-022-24077-3.

[76] Fraunhofer Ise and Pse Projects GmbH. *Solar PV Global Supply Chains*. Licence: CC BY 4.0. 2022. URL: https://www.iea.org/reports/solar-pv-global-supply-chains.

[77] Wikipedia. *Monocrystalline silicon*. URL: https://en.wikipedia.org/wiki/Monocrystalline_silicon. (Accessed August 17, 2024).

[78] Tadiran Batteries. *Products*. URL: https://tadiranbat.com/products/. (Accessed May 7, 2024).

[79] Huahui Energy. *China Lithium Titanate Battery*. URL: https://www.huahuibattery.com/supplier-3069368-lithium-titanate-battery. (Accessed July 29, 2024).

[80] Association des Constructeurs Européens d’Automobiles (ACEA). *Alternatively-powered vehicles (APV)*. URL: www.acea.auto.

[81] Maks Merela and Katarina Čufar. "Mechanical properties of sapwood versus heartwood, in three different oak species". In: *Drvna Industrija* 64 (4 2013), pp. 323–334. ISSN: 00126772. DOI: 10.5552/drind.2013.1325.

[82] Wikipedia. *Corrugated fiberboard*. URL: https://en.wikipedia.org/wiki/Corrugated_fiberboard. (Accessed July 24, 2024).

[83] Council of the EU. *Euro 7: Council adopts new rules on emission limits for cars, vans and trucks*. 12 April 2024. URL: https://www.consilium.europa.eu/en/press/press-releases/2024/04/12/euro-7-council-adopts-new-rules-on-emission-limits-for-cars-vans-and-trucks/.

[84] Parc naturel régional de la Sainte-Baume. URL: https://www.pnr-saintebaume.fr/. (Accessed July 28, 2024).

[85] SUZUKI France. *L'Office National des Forêts adopte l'Ignis Hybrid Suzuki*. URL: https://www.suzuki.fr/actualites/loffice-national-des-forets-adopte-lignis-hybrid-suzuki. (Accessed July 24, 2024).

[86] Elisabeth Weymar and Matthias Finkbeiner. "Statistical analysis of empirical lifetime mileage data for automotive LCA". In: *International Journal of Life Cycle Assessment* 21 (2 Feb. 2016), pp. 215–223. ISSN: 16147502. DOI: 10.1007/s11367-015-1020-6.

[87] Michael Ben-Chaim, Efraim Shmerling, and Alon Kuperman. "Analytic modeling of vehicle fuel consumption". In: *Energies* 6 (1 2013), pp. 117–127. ISSN: 19961073. DOI: 10.3390/en6010117.

[88] Wikipedia. *Diesel fuel*. URL: https://en.wikipedia.org/wiki/Diesel_fuel. (Accessed July 26, 2024).

[89] Ukpanah Inemesit. *Global Solar Energy Trends in 2024: Facts and Forecasts*. URL: https://www.greenmatch.co.uk/solar-energy/solar-pv-statistics. (Accessed August 15, 2024).

[90] Wikipedia. *Planetary boundaries*. URL: https://en.wikipedia.org/wiki/Planetary_boundaries. (Accessed August 15, 2024).

[91] Serenella Sala et al. "Environmental sustainability of European production and consumption assessed against planetary boundaries". In: *Journal of Environmental Management* 269 (Sept. 2020). ISSN: 10958630. DOI: 10.1016/j.jenvman.2020.110686.

[92] Wikipedia. *Var (department)*. URL: https://en.wikipedia.org/wiki/Var_(department). (Accessed August 15, 2024).

[93] Worldometer. *World Population by Year*. URL: https://www.worldometers.info/world-population/world-population-by-year/. (Accessed August 15, 2024).

[94] Statista. *Total forest area worldwide from 1990 to 2021.* URL: https://www.statista.com/statistics/1292175/global-forest-area/#:~:text=Forests%20cover%20over%20four%20billion,4.24%20billion%20hectares%20in%201990.. (Accessed March 17, 2024).

[95] Firechief® Global Matt Humby. *Lithium-ion batteries: a growing fire risk.* URL: https://www.britsafe.org/safety-management/2024/lithium-ion-batteries-a-growing-fire-risk. (Accessed March 18, 2024).

[96] (c) 2024 Tesla-Fire.com. *Tesla Fire records information about Tesla car fires and other Tesla fire incidents that received news coverage.* URL: https://www.tesla-fire.com/. (Accessed August 13, 2024).

[97] IMPACT FIRE. *How Do You Put Out a Lithium-Ion Battery Fire?* 2021. URL: https://resources.impactfireservices.com/how-do-you-put-out-lithium-ion-battery-fire. (Accessed August 13, 2024).

[98] Thompson Safety. *How Do You Put Out A Lithium-Ion Battery Fire?* URL: https://thompson-safety.com/company/press/lithium-ion-battery-fire. (Accessed August 13, 2024).

[99] Francesco Del Pero, Massimo Delogu, and Marco Pierini. "Life Cycle Assessment in the automotive sector: A comparative case study of Internal Combustion Engine (ICE) and electric car". In: *Procedia Structural Integrity.* Vol. 12. Elsevier B.V., 2018, pp. 521–537. DOI: 10.1016/j.prostr.2018.11.066.

[100] © 2024 Ecochain Technologies. *Impact Categories (LCA) – The complete overview.* URL: https://ecochain.com/blog/impact-categories-lca/. (Accessed March 17, 2024).

UNIVERSITÉ CATHOLIQUE DE LOUVAIN
École polytechnique de Louvain
Rue Archimède, 1 bte L6.11.01, 1348 Louvain-la-Neuve, Belgique | **www.uclouvain.be/epl**